

Jmjd2c facilitates the assembly of essential enhancer-protein complexes at the onset of embryonic stem cell differentiation

Rute A. Tomaz¹, Jennifer L. Harman², Donja Karimlou¹, Lauren Weavers¹, Lauriane Fritsch³, Tony Bou-Kheir¹, Emma Bell¹, Ignacio del Valle Torres⁴, Kathy K. Niakan⁴, Cynthia Fisher⁵, Onkar Joshi⁶, Hendrik G. Stunnenberg⁶, Edward Curry¹, Slimane Ait-Si-Ali³, Helle F. Jørgensen² and Véronique Azuara^{1,*}

ABSTRACT

Jmjd2 H3K9 demethylases cooperate in promoting mouse embryonic stem cell (ESC) identity. However, little is known about their importance at the exit of ESC pluripotency. Here, we reveal that Jmjd2c facilitates this process by stabilising the assembly of mediator-cohesin complexes at lineage-specific enhancers. Functionally, we show that Jmjd2c is required in ESCs to initiate appropriate gene expression programs upon somatic multi-lineage differentiation. In the absence of Jmjd2c, differentiation is stalled at an early post-implantation epiblast-like stage, while *Jmjd2c*-knockout ESCs remain capable of forming extra-embryonic endoderm derivatives. Dissection of the underlying molecular basis revealed that Jmjd2c is re-distributed to lineage-specific enhancers during ESC priming for differentiation. Interestingly, Jmjd2c-bound enhancers are co-occupied by the H3K9-methyltransferase G9a (also known as Ehmt2), independently of its H3K9-modifying activity. Loss of Jmjd2c abrogates G9a recruitment and further destabilises loading of the mediator and cohesin components Med1 and Smc1a at newly activated and poised enhancers in ESC-derived epiblast-like cells. These findings unveil Jmjd2c and G9a as novel enhancer-associated factors, and implicate Jmjd2c as a molecular scaffold for the assembly of essential enhancer-protein complexes with an impact on timely gene activation.

KEY WORDS: Jmjd2c (Kdm4c), Enhancers, Gene regulation, Embryonic stem cells, Epiblast stem cells, Lineage specification

INTRODUCTION

Pluripotency, the ability of a cell to generate all somatic lineages, is transiently acquired *in vivo* during mammalian pre-implantation development. Upon blastocyst formation, pluripotent cells develop within the inner cell mass (ICM), a mosaic of cells surrounded by an extra-embryonic layer – the trophectoderm. By the time of

implantation, a second extra-embryonic lineage, the primitive endoderm, emerges at the ICM surface. Concurrently, the ICM maintains its pluripotency as it matures into the epiblast but ultimately goes on to form the three primary germ layers and germ cells upon gastrulation (Boroviak and Nichols, 2014; Rossant, 2008).

Pluripotent mouse embryonic stem cells (ESCs) are derived from ICM cells, and can self-renew and faithfully maintain an undifferentiated state *in vitro* in the presence of leukaemia inhibitory factor (LIF) and serum components, while preserving their multi-lineage differentiation capacity (Evans and Kaufman, 1981; Martin, 1981; Niwa et al., 1998; Ying et al., 2003). Most recently, stem cell lines with similar lineage potential were established from other developmental stages (Chung et al., 2006; Tesar, 2005), including a number of post-implantation epiblast-derived stem cells (EpiSCs) (Brons et al., 2007; Osorno et al., 2012; Tesar et al., 2007). While ESCs are thought to represent an immature (pre-implantation) phase of pluripotency, EpiSCs exist in a more advanced state on the verge of differentiation (Nichols and Smith, 2009). Moreover, ESCs can stably transit into self-renewing EpiSCs, acquiring characteristics of post-implantation epiblast-like cells (Guo et al., 2009).

ESC abilities depend on the potent expression of self-renewal genes and transcriptional priming of silent, lineage-affiliated genes – a crucial balance of gene expression maintained through crosstalk between transcriptional factors and chromatin regulators (Azuara et al., 2006; Bernstein et al., 2006; Chen and Dent, 2014; Ng and Surani, 2011; Stock et al., 2007). Remarkably, both active (ESC-specific) and primed (lineage-specific) genes are expressed in a heterogeneous manner, a feature long considered to be a hallmark of ESC cultures that safeguards the swift response to differentiation cues (Efroni et al., 2008; Torres-Padilla and Chambers, 2014). Yet, it is now possible to derive and maintain ESCs with reduced heterogeneity and transcriptional gene priming through chemical inhibition of two differentiation-associated pathways, Mek and Gsk3 (2i conditions), capturing a naïve pluripotent state *in vitro* (Marks et al., 2012; Ying et al., 2008).

Gene promoter regions enriched in CpG islands and H3K4me3 function as genomic platforms for the recruitment of transcription factors and co-regulators, as well as for the basal transcriptional machinery (Deaton and Bird, 2011; Illingworth and Bird, 2009). Moreover, distal DNA elements such as enhancers play a significant role in potentiating gene expression being typically decorated by H3K4me1 and bound by pioneer transcription factors (Calo and Wysocka, 2013; Gibcus and Dekker, 2013; Spitz and Furlong, 2012). For example, the core pluripotency factor Oct4 was commonly shown to mark both active and poised enhancers in ESCs and EpiSCs (Buecker et al., 2014; Calo and Wysocka, 2013). Enhancer activity and robust ESC-specific gene expression entail long-range DNA interactions with the transcriptional apparatus at

¹Institute of Reproductive and Developmental Biology, Faculty of Medicine, Imperial College London, London W12 0NN, UK. ²Cardiovascular Medicine Division, Department of Medicine, University of Cambridge, Cambridge CB2 0QQ, UK. ³Centre National de la Recherche Scientifique CNRS - Université Paris Diderot, Sorbonne Paris Cité, Epigenetics and Cell Fate, UMR 7216 CNRS, Paris 75013, France. ⁴Human Embryo and Stem Cell Laboratory, The Francis Crick Institute, London NW7 1AA, UK. ⁵Wellcome Trust Sanger Institute, Hinxton, Cambridge CB10 1HH, UK. ⁶Radboud University, Faculty of Science, Department of Molecular Biology, Nijmegen 6525GA, The Netherlands.

*Author for correspondence (v.azuara@imperial.ac.uk)

 R.A.T., 0000-0002-9377-1431; V.A., 0000-0003-4608-3713

This is an Open Access article distributed under the terms of the Creative Commons Attribution License (<http://creativecommons.org/licenses/by/3.0>), which permits unrestricted use, distribution and reproduction in any medium provided that the original work is properly attributed.

promoters, involving the cooperative action of mediator-cohesin complexes (Kagey et al., 2010). Yet, relatively little is known about the identity of proteins that stabilise the formation of such assemblies.

Histone demethylases have emerged as key players in the control of cell identity and development, mainly through modulation of the chromatin environment of tissue-specific genes (Nottke et al., 2009). Recently, additional roles for these molecules independent of their enzymatic activity have been reported (Shpargel et al., 2012; Wang et al., 2012; Yang et al., 2010), especially in regulating the recruitment of Polycomb repressive complexes (PRC) and poised RNA polymerase II to the promoter regions of developmental genes in ESCs (Farcas et al., 2012; Wu et al., 2013). *Jmjd2c* (also known as *Kdm4c*) is a member of the *Jmjd2* gene family initially identified as H3K9me2/3 and/or H3K36me2/3 histone demethylases (Chen et al., 2006; Klose et al., 2006; Whetstine et al., 2006). *Jmjd2c* is highly expressed in the early embryo and in ESCs (Boroviak et al., 2015; Burton et al., 2013; Loh et al., 2007; Wang et al., 2010), and RNA interference-mediated depletion of the protein was shown to impair cleavage-stage development and ESC integrity, as well as inhibiting somatic cell reprogramming (Das et al., 2014; Loh et al., 2007; Wang et al., 2010). *Jmjd2c*-null ESCs and mice could, however, be generated via gene trap approaches (Pedersen et al., 2014), in agreement with functional redundancy between *Jmjd2* gene family members to support cell proliferation and survival (Pedersen et al., 2016). At the genomic level, *Jmjd2c* preferentially targets H3K4me3-rich promoter regions of active and development-associated genes in ESCs via its Tudor domains (Das et al., 2014; Pedersen et al., 2014), where *Jmjd2c* is proposed to assist *Jmjd2b*-Nanog and PRC2 in transcriptional activation and repression, respectively (Das et al., 2014).

In this study, we uncover a previously unrecognised link between *Jmjd2c* recruitment to lineage-specific enhancers and the establishment of a functionally primed state for differentiation *in vitro*. We show that, in the absence of *Jmjd2c*, ESC differentiation is severely impeded at an early post-implantation epiblast-like stage. Although *Jmjd2c*-knockout ESCs can transit into self-renewing EpiSCs, these cells fail to form derivatives of the three primary germ layers, as revealed by their inability to initiate appropriate gene expression programs. By contrast, *Jmjd2c*-knockout cells remain capable of adopting extra-embryonic endoderm-like phenotypes under permissive conditions. Mechanistically, we show that *Jmjd2c* is re-distributed to lineage-specific enhancers in primed (serum/LIF) as opposed to naïve (2i/LIF) ESCs. Strikingly, *Jmjd2c*-bound enhancers are co-occupied by the antagonistic enzyme G9a (also known as Ehmt2), independently of its silencing H3K9-modifying activity. We show that *Jmjd2c* and G9a co-occupancy coincides with the formation of activating, Med1-containing enhancer complexes. Loss of *Jmjd2c* abrogates G9a recruitment at *Jmjd2c*-bound distal sites, which correlates with inefficient loading of mediator-cohesin complexes in ESC-derived EpiSCs and impacts on gene activation upon lineage specification. Collectively, these data reveal that *Jmjd2c* is required for successful gene transcription and somatic differentiation in pluripotent stem cells, and propose a novel regulatory role for *Jmjd2c* in stabilising the assembly of essential enhancer-protein complexes at the onset of ESC differentiation.

RESULTS

Jmjd2c is required for embryonic stem cell differentiation towards somatic lineages

Combining genetic deletion and functional assays, we tested whether *Jmjd2c* plays a role at the exit of pluripotency. *Jmjd2c*

mutant and wild-type JM8-ESCs were obtained through the EUCOMM/IKMC repository (Bradley et al., 2012; Skarnes et al., 2011), and targeting of both *Jmjd2c* alleles in *Jmjd2c*-knockout (E2 and E3) ESC clones was confirmed by long-range PCR and GFP expression (Fig. S1A–C). Western blotting validated that full-length *Jmjd2c* protein expression was completely abolished in *Jmjd2c*-knockout samples (Fig. 1A). This was accompanied by a notable increase in bulk H3K9me2 levels relative to wild type (Fig. 1B, Fig. S1D), an effect attributed to the loss of *Jmjd2c* itself in the continued expression of other H3K9 demethylases and methyltransferases (Fig. S1D,E). Constitutively *Jmjd2c*-depleted E2 and E3 ESC clones grew normally in medium supplemented with serum plus LIF (Fig. S1F), in agreement with a similar conditional knockout model (Pedersen et al., 2014). When plated at low density, these cells also displayed comparable proportion of undifferentiated colonies relative to their wild-type counterparts (Fig. 1C), despite reduced expression levels of pluripotency-associated factors (Fig. S1G). *Jmjd2c* depletion did not, however, result in general de-repression of differentiation-associated genes (Fig. S1H), including those co-bound by *Jmjd2c* and PRC complexes at their promoter regions (Das et al., 2014). These data indicate that constitutive *Jmjd2c*-knockout ESCs retain a self-renewing and undifferentiated phenotype in pluripotency culture conditions.

To assess the effect of *Jmjd2c* deficiency on differentiation, *Jmjd2c*-knockout and wild-type ESCs were induced to form embryoid bodies (EBs) (Fig. 1D,E). In contrast to the dispensability of *Jmjd2c* for ESC self-renewal, *Jmjd2c*-deficient cells were unable to properly differentiate into derivatives of the three germ layers. These cells formed smaller EBs (Fig. 1D) that, in contrast to wild-type EBs, showed residual expression of the pluripotency factors *Oct4* and *Nanog* (Fig. 1E, upper panel). Notably, *Jmjd2c*-knockout EBs showed impaired expression of the epiblast marker *Fgf5* and several mesoderm, endoderm and ectoderm germ layer-affiliated genes (Fig. 1E, lower panels). Importantly, this defect was recapitulated using another loss-of-function strategy (Fig. S2). Using validated puromycin-selectable shRNA vectors (Loh et al., 2007), we could indeed stably establish several *Jmjd2c*-knockdown E14-ESC clones (Fig. S2A–C). As *Jmjd2c*-knockout ESCs, these clones proliferated normally, showing no incidence of spontaneous differentiation and/or prominent gene de-repression (Fig. S2D,E). Moreover, we found that *Jmjd2c*-knockdown ESCs failed to potently activate brachyury and *Mixl1* upon EB formation, despite evidence for *Fgf5* induction at variable levels in different clones and experiments (Fig. S2F; data not shown). Collectively, these findings demonstrate that *Jmjd2c* is important for the successful differentiation of ESCs into multiple somatic lineages.

Strikingly, however, *Jmjd2c*-deficient cells could differentiate upon LIF withdrawal and addition of all-trans retinoic acid (atRA), indicating that not all differentiation pathways in ESCs were compromised in the absence of *Jmjd2c*. Differentiation was evidenced by a complete loss of *Oct4* expression (Fig. 1F), and prominent upregulation of *Gata6*, *Gata4*, *Sox7* and *Dab2* transcripts (Fig. 1G), consistent with the preferential acquisition of a primitive endoderm (PrE)-like phenotype under these conditions (Artus et al., 2010; Capo-Chichi et al., 2005). In atRA-treated wild-type ESCs, PrE-like differentiation was marked by the swift downregulation of *Jmjd2c* (Fig. 1G, bottom panel), similar to what was observed upon trophoblast lineage commitment *in vitro* (Alder et al., 2010). These findings corroborate with *in vivo* studies showing that *Jmjd2c* expression

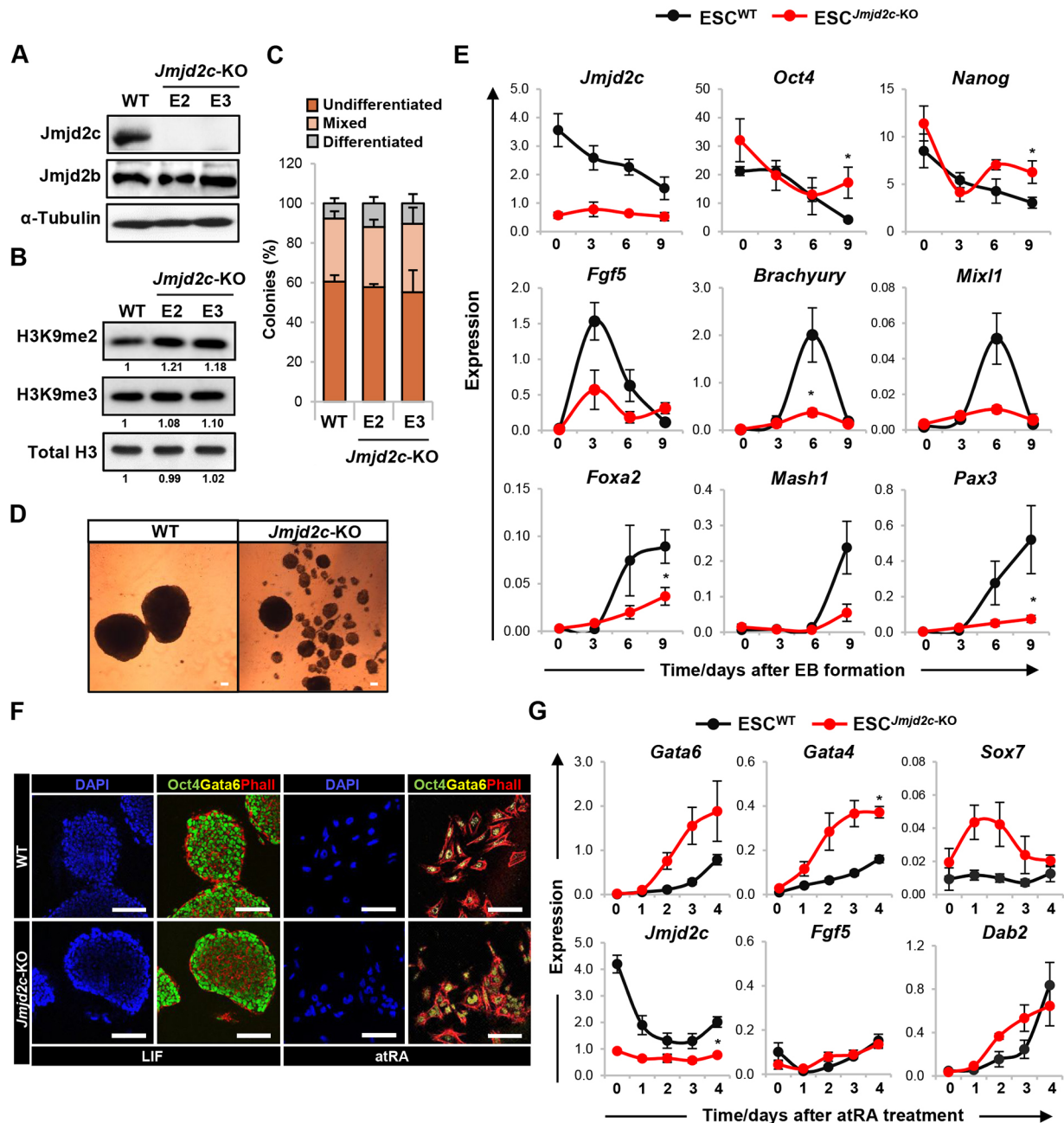


Fig. 1. *Jmjd2c*-knockout ESCs can self-renew but fail to differentiate into somatic lineages. (A) Western blot using anti-Jmjd2c and anti-Jmjd2b antibodies of whole-cell extracts from wild-type (WT) JM8-ESCs and *Jmjd2c*-knockout (*Jmjd2c*-KO) cell lines (E2 and E3). α -Tubulin is used as loading control. (B) Western blots showing bulk levels of H3K9me2, H3K9me3 and total histone H3 in acid-extracted histone lysates from wild-type and *Jmjd2c*-KO cells. Signal quantification is presented relative to wild type. (C) Ability of wild-type and *Jmjd2c*-KO cells to self-renew. Cells were plated at low density and cultured for 5 days with LIF. Colonies were scored as undifferentiated, mixed or differentiated based on alkaline phosphatase activity. Data represent mean \pm s.e.m. of four experiments. (D) Phase-contrast images of day 9 embryoid bodies (EBs) formed from wild-type and *Jmjd2c*-KO (E3) ESCs. Scale bars: 100 μ m. (E) Expression profiling of *Jmjd2c*, pluripotency-associated (*Nanog*, *Oct4*), epiblast (*Fgf5*), mesoderm (*brachyury*, *Mixl1*), endoderm (*Foxa2*) and neuroectoderm (*Mash1*, *Pax3*) markers during EB-mediated differentiation, as assessed by RT-qPCR and normalised to housekeeping genes. Data represent mean \pm s.e.m. of at least three experiments. * P < 0.05; Mann-Whitney U -test at peak time-points. (F) Immunofluorescence staining for Oct4 (green), Gata6 (yellow) and phalloidin (red) in wild-type and *Jmjd2c*-KO (E3) ESCs maintained under proliferative conditions or upon 1 μ M retinoic acid (atRA) addition and LIF removal for 4 days. Scale bars: 100 μ m. (G) Transcript levels of *Gata6*, *Gata4*, *Sox7* and *Dab2* (PrE markers), *Jmjd2c* and *Fgf5*, as assessed during atRA-induced differentiation. Expression is normalised to housekeeping genes and data show mean \pm s.e.m. of three experiments. * P < 0.05; Mann-Whitney U -test at day 4.

is dynamically lost in the primitive endoderm, while being retained in the epiblast of peri-implantation embryos (Fig. S3) (Boroviak et al., 2015; Burton et al., 2013). Hence, *Jmjd2c* might be expendable for the formation of extra-embryonic lineages where it is not normally expressed, an observation that was

substantiated by the successful generation of extra-embryonic endoderm (XEN) stem cells from *Jmjd2c*-knockout ESCs (Fig. S4) (Cho et al., 2012; Kunath et al., 2005; Niakan et al., 2013). Collectively, our results support a selective requirement for *Jmjd2c* during epiblast-derived lineage specification.

Lack of transcriptional gene priming and skewed cell fate in *Jmjd2c*-deficient epiblast stem cells

To explore the timing of *Jmjd2c* function in somatic differentiation, we first examined whether *Jmjd2c* was required during the transition from ESC to EpiSC pluripotent states (Guo et al., 2009). Both *Jmjd2c*-knockout and wild-type EpiSC lines could be stably established (Fig. S5). However, during this process, we noticed a delay in the induction of the early EpiSC markers *Otx2* and *Dnmt3b* (Tesar et al., 2007; Veillard et al., 2014) in *Jmjd2c*-knockout relative to wild-type ESCs when treated with activin and fibroblast growth factor (Fig. S5A). Notably, lower *Fgf5* mRNA levels were detected in stably converted EpiSCs (cEpiSCs) in the absence of *Jmjd2c*. Hence, although *Jmjd2c*-deficient ESCs retain the ability to convert into EpiSCs, these cells harbour an incomplete/immature epiblast-like state, which is further suggested by a lack of low-level transcripts at primed germ layer (brachyury and *Foxa2*) markers in *Jmjd2c*-knockout cEpiSCs (Fig. S5A, lower panel).

To determine whether *Jmjd2c* deficiency also impacts on the ability of cEpiSCs to respond to differentiation cues, we compared the behaviour of *Jmjd2c*-knockout and wild-type cEpiSCs when prompted to differentiate towards mesodermal lineages. Here, we used a protocol adapted from a human ESC differentiation model

(Cheung et al., 2012) to induce early mesodermal (EM) progenitors and mature lateral plate mesodermal (LPM) and paraxial mesodermal (PM) cell types (Fig. 2A). Both control EpiSCs and wild-type cEpiSCs readily acquired an EM-like identity, as typified by the loss of *Fgf5* expression and acquisition of the early primitive streak marker brachyury at day 1–1.5 post-induction (Fig. 2B). By contrast, we found that *Jmjd2c*-knockout cEpiSCs were unable to efficiently progress into early, brachyury-positive, mesodermal progenitors, confirming that differentiation blockage occurs at an early epiblast-like stage in the absence of *Jmjd2c*.

All three cell lines were further differentiated under LPM and PM conditions, generating Flk1- and *Pdgfra*-expressing cell populations, respectively, as monitored by flow cytometry on day 4 post-induction (Fig. 2C). Although the wild-type cEpiSC response closely mirrored that of embryo-derived EpiSCs, differentiation into mature cell types was blocked in *Jmjd2c*-knockout cultures, showing impaired expression of LPM (*Kdr/Flk1* and *Isl1*) and PM (*Pdgfra* and *Meox1*) markers. Instead, and irrespective of LPM and PM conditions, *Jmjd2c*-knockout cells induced typical post-implantation extra-embryonic endoderm (*Lrp2* and *Sparc*) but not definitive and pan endodermal (*Cxcr4* and *Foxa2*) markers (Fig. 2D, right panels). Moreover, these cells

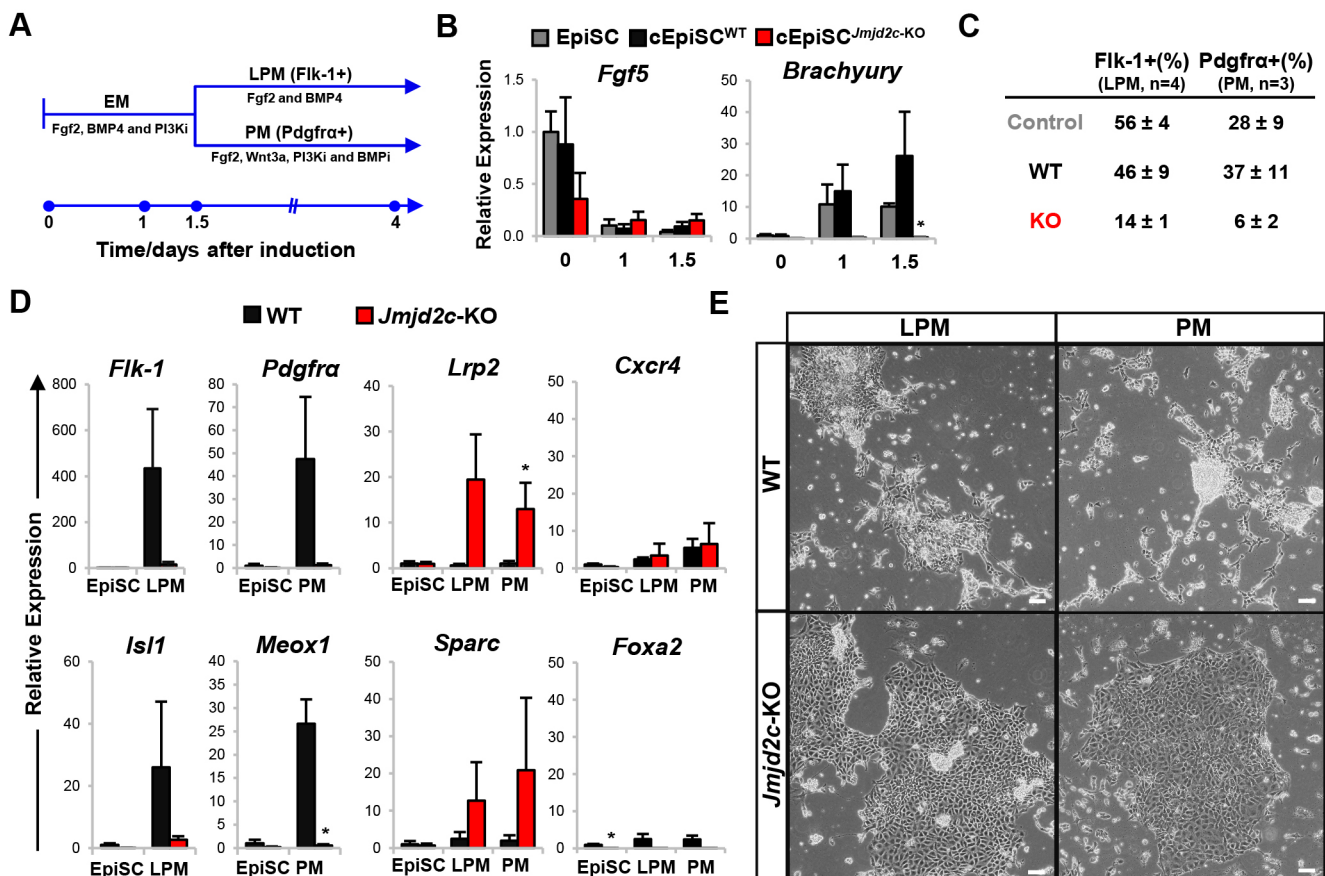


Fig. 2. Skewed differentiation of *Jmjd2c*-knockout cEpiSCs upon mesoderm induction. (A) Timeline of EpiSC induction towards early mesodermal (EM) progenitors and mature lateral plate mesoderm (LPM) and paraxial mesoderm (PM) cells. (B) Expression levels of *Fgf5* and brachyury in control embryo-derived EpiSCs (grey), wild-type (black) and *Jmjd2c*-KO (red) cEpiSCs upon EM induction. Data are normalised to housekeeping genes and expressed relative to control EpiSCs as mean \pm s.e.m. of three experiments. * $P < 0.05$; Mann–Whitney *U*-test. (C) Average percentage (\pm s.e.m.) of Flk1-positive LPM and *Pdgfra*-positive PM differentiated cells, as monitored by flow cytometry in control, wild-type and *Jmjd2c*-KO cultures at day 4 post-induction in at least three experiments. (D) Expression of lateral plate (*Kdr/Flk1* and *Isl1*) and paraxial (*Pdgfra* and *Meox1*) mesoderm; extra-embryonic endoderm (*Lrp2* and *Sparc*); and definitive (*Cxcr4*) and pan (*Foxa2*) endoderm markers in wild-type and *Jmjd2c*-KO differentiated cells under LPM/PM conditions. Data are normalised to housekeeping genes and expressed relative to wild type (day 0) as mean \pm s.e.m. of three experiments. * $P < 0.05$; Mann–Whitney *U*-test. (E) Phase-contrast images of LPM and PM wild-type and *Jmjd2c*-KO cultures. Scale bars: 100 μ m.

acquired an adhesive, polarised epithelium-like morphology (Fig. 2E) and stained positive for E-cadherin (Fig. S6) similar to what is observed upon BMP4-induced differentiation of XEN cells (Artus et al., 2012; Paca et al., 2012). Collectively, our findings suggest that, in the absence of Jmjd2c, epiblast cell fate might default towards extra-embryonic endoderm-like derivatives, as tested here upon mesodermal lineage induction.

De novo Jmjd2c recruitment to H3K4me1/me2-rich lineage-specific enhancers in primed embryonic stem cells

We have shown that *Jmjd2c* loss in ESCs is sufficient to inhibit somatic differentiation, despite *Jmjd2c* being normally downregulated upon induction (Fig. 1E, upper panel). This suggests an important role for Jmjd2c in undifferentiated ESCs either in preserving their multi-lineage potential or in mediating the transition from pluripotent ESC to differentiated states. To address the molecular basis for the skewed differentiation of *Jmjd2c*-knockout ESCs, we mapped and compared Jmjd2c DNA-binding sites by ChIP-seq in naïve (2i/LIF) and primed (serum/LIF) ESCs (Marks et al., 2012). To achieve this, E14-ESC clones stably expressing Flag-tagged Jmjd2c were generated (ESC^{FV-Jmjd2c-WT}, Fig. S7), and expanded in either condition prior to anti-Flag ChIP (Fig. S8A,B).

In 2i/LIF, over 70% of Jmjd2c peaks were detected within 1 kb of the transcriptional start sites (TSS) (Fig. 3A), as previously reported (Pedersen et al., 2014). Strikingly, however, Jmjd2c genomic distribution was altered during the priming of ESCs for differentiation. Substantially more Jmjd2c peaks (45,485 versus 20,377; FDR<0.0001) were detected in serum/LIF relative to 2i/LIF conditions. Moreover, we found that the majority of the peaks specific to the serum/LIF state were located more than 1 kb away from the TSS interval, hereafter referred to as distal peaks (Fig. 3A; Fig. S8C). This trend was recapitulated by interrogating an independent ChIP-seq dataset (Fig. S8D) (Das et al., 2014). Importantly, we identified that the sets of genes targeted by Jmjd2c in the two ESC states were largely overlapping, as revealed using gene annotation analysis (Fig. 3B). Hence, these findings uncover that, in 2i/LIF, Jmjd2c primarily binds to TSS regions, yet additionally occupies distal regions affiliated with the same cohort of genes in serum/LIF, as further validated at selected (*Fgf5* and *brachyury*) loci by ChIP-qPCR on endogenous Jmjd2c protein in naïve (2i/LIF) and primed (serum/LIF) wild-type and *Jmjd2c*-knockout ESCs (Fig. S8E–G).

Jmjd2c-bound distal peaks most closely overlapped with H3K4me1-rich sites (Fig. 3C), which typically define enhancers (Creyghton et al., 2010; Zentner et al., 2011). As expected, Jmjd2c-bound TSS regions were preferentially decorated with H3K4me3, whereas H3K4me2 could be detected at both TSS and distal peaks. Given that Jmjd2c can bind both H3K4me2 and H3K4me3 in a Tudor domain-dependent manner (Pedersen et al., 2014), we asked whether Jmjd2c recruitment at enhancers might be at least partly mediated via H3K4me2 recognition. Combining mutagenesis and ChIP-qPCR analyses, we showed that Jmjd2c binding was abrogated at TSS and distal regions in ESCs expressing a mutant version of Jmjd2c lacking its two Tudor domains (ESCs^{FV-Jmjd2c-ΔT}) (Fig. 3D; Fig. S7D), indirectly validating H3K4-dependent Jmjd2c DNA binding. Strikingly, however, FV-Jmjd2c-ΔT binding was selectively retained at ESC-specific (*Esrrb* and *Klf4*) enhancers (Fig. 3D, bottom panel), suggesting a different mode of Jmjd2c recruitment at these sites possibly via cooperation with additional enhancer-bound proteins, including Jmjd2b and Nanog, as previously suggested (Das et al., 2014).

Active and poised enhancers can be distinguished genome-wide by the presence or absence of p300-mediated H3K27ac marks (Creyghton et al., 2010; Zentner et al., 2011). Interestingly, we found that 85% of Jmjd2c-bound distal peaks harboured low or no H3K27ac deposition (Fig. 3E), indicating that Jmjd2c is prevalently recruited to poised enhancers in serum/LIF. Known motif sequence enrichment analysis at these sites disclosed a high incidence of motifs for differentiation-associated factors, such as brachyury, Gata3 and Atoh1 (Fig. 3F), typifying tissue-specific enhancers activated later on during development. Concordantly, Gene Ontology analysis revealed significant enrichment for developmental and somatic differentiation processes at Jmjd2c-bound, H3K27ac-low sites (Fig. 3G). These findings support a role for Jmjd2c in promoting differentiation into derivatives of the three primary germ layers. Taken together, our findings reveal that Jmjd2c is recruited in a timely manner to lineage-specific enhancers during ESC priming for differentiation.

The antagonistic enzymes Jmjd2c and G9a are co-enriched at active and poised enhancers independently of H3K9-modifying activities

Consistent with its H3K9-demethylase activity (Cloos et al., 2006; Whetstone et al., 2006), we showed that constitutively depleting Jmjd2c in ESCs leads to a noticeable increase in bulk H3K9me2 levels (Fig. 1B, Fig. S1D). Deposition of H3K9 and DNA methylation are known mechanisms operating in extra-embryonic tissues and derived stem cells to prevent the expression of somatic, lineage-specific genes (Alder et al., 2010; Senner et al., 2012). In light of the skewed differentiation of *Jmjd2c*-knockout ESCs towards extra-embryonic fates, we thus asked whether Jmjd2c occupancy might antagonise the acquisition of repressive marks in pluripotent stem cells.

At the chromosomal level, G9a-mediated H3K9me2 deposition encompasses large domains yet is depleted at the TSS regions of active and lineage-specific genes in ESCs (Lienert et al., 2011). We confirmed genome-wide that Jmjd2c and H3K9me2 are mutually exclusive across Jmjd2c-bound TSS regions, whereas G9a and H3K9me2 are confined to regions flanking Jmjd2c peak summits, as demonstrated using heatmap distributions and Pearson's correlation coefficients (Fig. 4A,B, left panels). In striking contrast, however, Jmjd2c and G9a largely overlapped across enhancer regions in the absence of H3K9me2 deposition (Fig. 4A,B, right panels), as observed at both active and poised Jmjd2c-bound distal sites (Fig. S9). The colocalisation of the two antagonistic enzymes Jmjd2c and G9a at enhancers suggests a possible counteracting mechanism in the control of gene expression. Loss of Jmjd2c, however, did not lead to increased levels of H3K9me2 and *de novo* DNA methylation (Fig. 4C; data not shown), as examined at the locus level across *Fgf5* and *brachyury* regulatory regions in *Jmjd2c*-knockout ESCs, and in derived cEpiSCs and induced-mesodermal progenitors where *Fgf5* and *brachyury* activation is respectively inhibited in the absence of Jmjd2c (Fig. 2). These data strongly suggest that, in contrast to what we hypothesised, the failure of *Jmjd2c*-knockout cells to differentiate towards somatic derivatives is not due to a lack of Jmjd2c-mediated protection against the acquisition of repressive marks at Jmjd2c-bound gene targets.

Surprisingly, we found that the highest levels of G9a were detected at active (H3K27ac-high) Jmjd2c-bound distal sites (Fig. S10A, left panel), as exemplified at *Esrrb* and *Klf4* loci (Fig. S10B,C). Moreover, G9a significantly overlapped with known enhancer-associated factors, including p300, Oct4 and the subunits

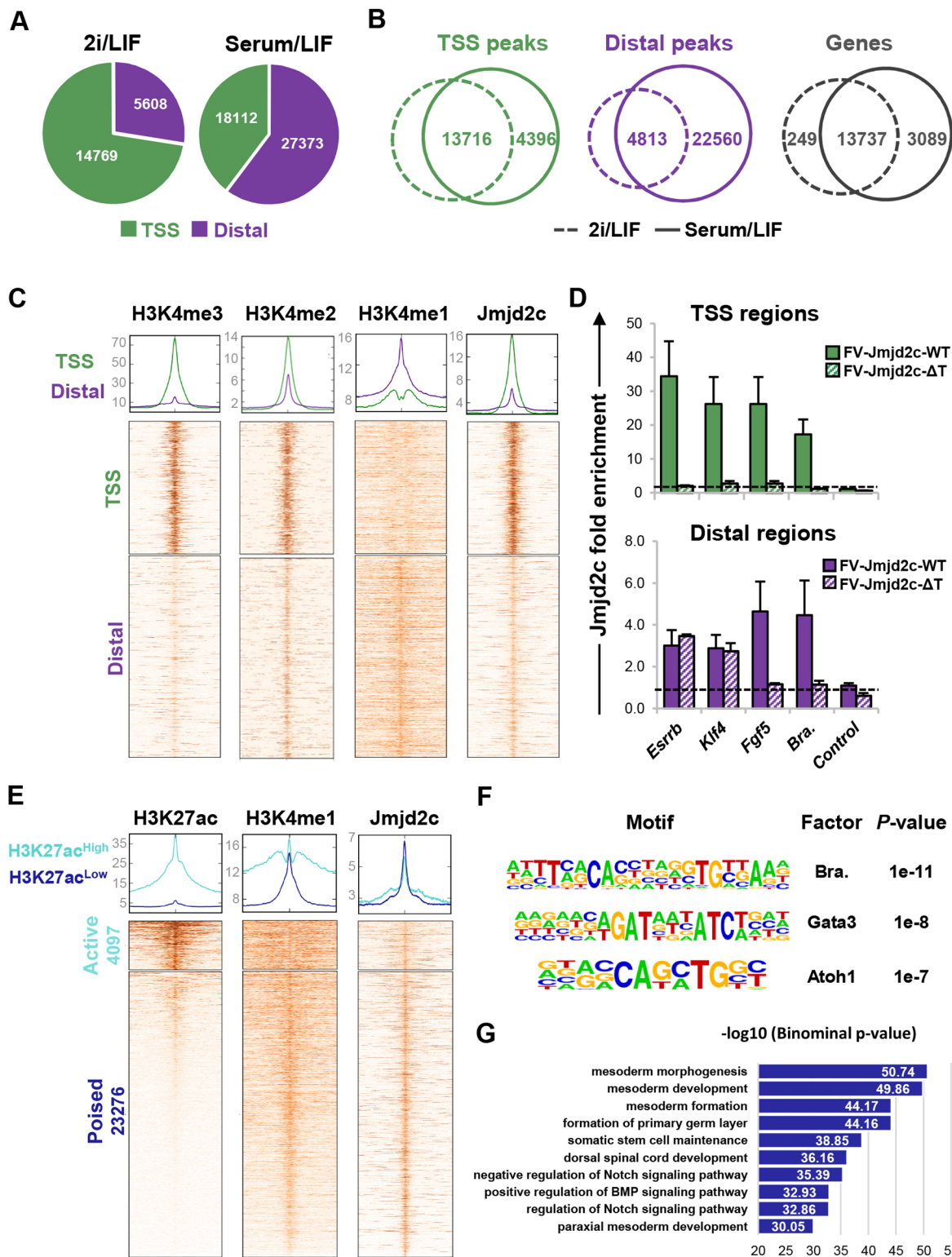


Fig. 3. Jmjd2c preferentially overlaps with H3K4me1/me2-rich lineage-specific enhancers in primed ESCs. (A) Numbers of Jmjd2c peaks located within 1 kb of transcriptional start sites (TSS) or outside this interval (distal) in 2i/LIF and serum/LIF. (B) Venn diagrams indicating the overlap of Jmjd2c-bound TSS and distal peaks in serum/LIF with at least one peak in 2i/LIF (minimum overlap=1 bp); overlap of the nearest gene to Jmjd2c peaks in the two conditions (right panel). (C) Density heatmaps of H3K4me3/2/1 and Jmjd2c levels across a 10 kb window centred at TSS and distal Jmjd2c-bound regions in serum/LIF. (D) Enrichment levels for full-length Jmjd2c (FV-Jmjd2c-WT) and a mutant form of Jmjd2c lacking Tudor domains (FV-Jmjd2c-ΔT) at TSS and enhancer sites of active (*Esrrb* and *Klf4*) and lineage-specific (*Fgf5* and brachyury) genes in ESCs. Fold enrichment is relative to control cells (empty vector; dotted line). Data represent mean±s.e.m. of three experiments. Background level is confirmed at an intergenic region. (E) Average density plots and heatmaps of H3K27ac, H3K4me1 and Jmjd2c levels across a 10 kb window centred at Jmjd2c-bound distal sites in serum/LIF. Peaks are sorted according to H3K27ac levels using a *k*-means clustering algorithm. (F) Motifs identified among overrepresented binding sequences at H3K27ac-low Jmjd2c distal peaks. (G) Top 10 most significant biological functions of genes associated with H3K27ac-low Jmjd2c distal peaks.

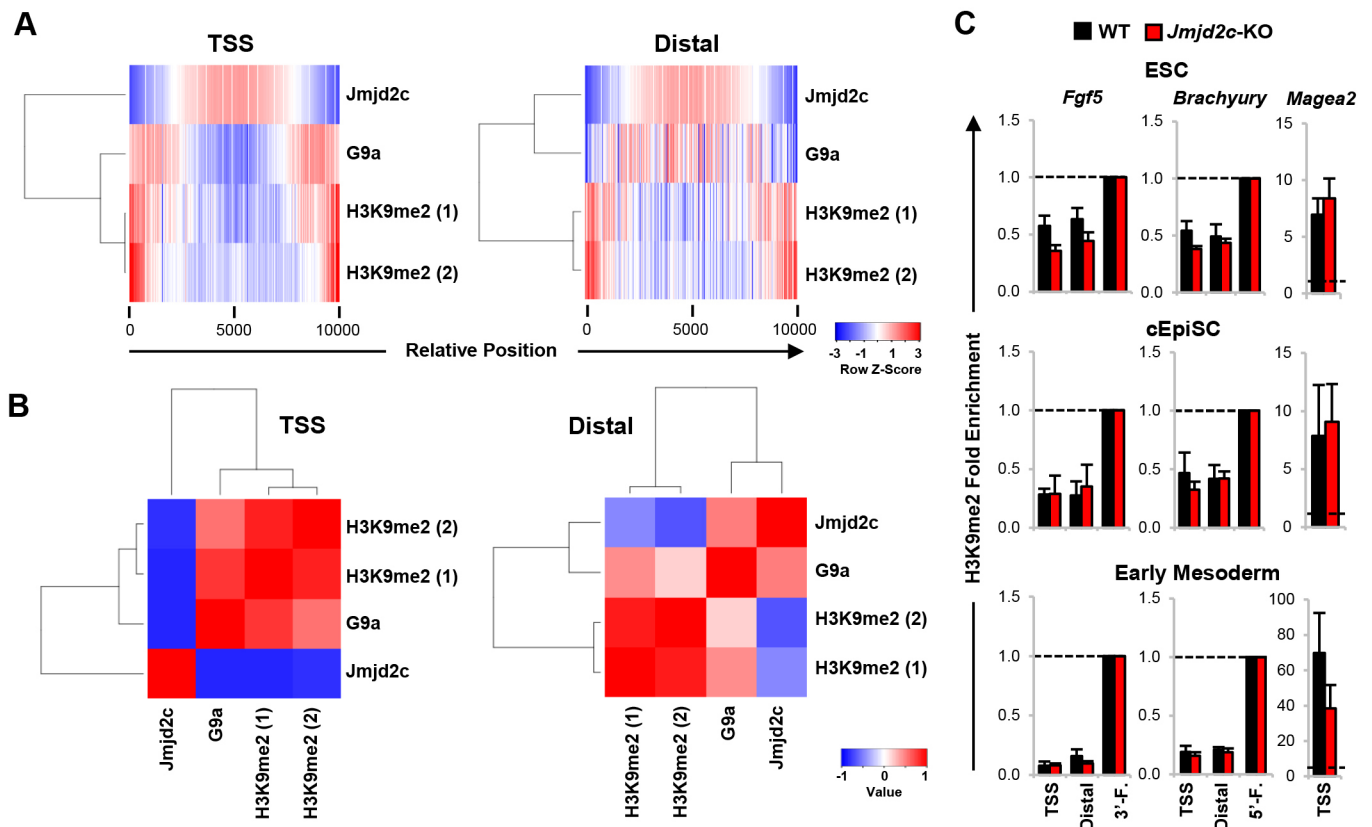


Fig. 4. G9a is enriched at distal Jmjd2c-bound sites independently of its H3K9-modifying activity. (A) Heatmap distributions (i.e. binned mean ChIP-seq read density) of Jmjd2c, G9a (Mozzetta et al., 2014), H3K9me2 (1) (Liu et al., 2015) and H3K9me2 (2) (Das et al., 2014) across Jmjd2c-bound TSS and distal sites. Each ChIP-seq experiment is adjusted for sequencing depth and normalised to respective input. Colour key indicates enrichment levels from low to high. (B) Heatmap showing Pearson correlation between Jmjd2c, G9a and H3K9me2 distributions across Jmjd2c-bound TSS and distal sites. Colour key indicates correlation coefficient from low to high. (C) Enrichment levels for H3K9me2 at TSS, distal/enhancer and Jmjd2c-free flanking regions of *Fgf5* and brachyury, as determined by ChIP-qPCR in wild-type and *Jmjd2c*-KO ESCs and cEpiSCs, and upon cEpiSC mesodermal induction. Data are relative to flanking regions (dotted line) and are shown as mean ± s.e.m. of three experiments. *Magea2* TSS is used as positive control.

of mediator (Med1) and cohesin (Smc1a) complexes at these sites in ESCs (Fig. 5A,B). Lower yet detectable G9a enrichment, with peaks closely aligned with Jmjd2c, p300, Oct4, Med1 and Smc1a, also marked poised (H3K27ac-low) Jmjd2c-bound enhancers (Fig. 5A, lower panels), as illustrated at *Fgf5* and brachyury loci (Fig. S10D-E). The detection of differential G9a enrichment levels at ESC-specific and transcriptionally primed loci was furthermore verified by ChIP-qPCR in JM8-ESCs (Fig. 5C), and validated in control and *G9a*-knockout ESCs, where G9a precipitation was abolished, as expected (Fig. S11A-C). Interestingly, although Jmjd2c binding remained unaltered in *G9a*-knockout ESCs, G9a was lost at *Fgf5* and brachyury enhancers in the absence of Jmjd2c (Fig. S11D), suggesting a possible role for Jmjd2c in facilitating G9a binding. Jmjd2c-G9a co-occupancy was furthermore supported by the identification of a physical interaction between Jmjd2c and G9a/GLP (Fig. 5D), and their simultaneous detection at the same enhancer fragments in sequential ChIP (re-ChIP) assays (Fig. S11E). Importantly, Jmjd2c and G9a also interact with Med1 (Fig. S11F-G), further implying that Jmjd2c-G9a co-occupancy might coincide with the assembly of activating protein mega-complexes at enhancers. Taken together, our findings unveil Jmjd2c and G9a as novel enhancer-associated factors, and demonstrate that these molecules are co-recruited genome-wide to active and poised enhancers in ESCs independently of their H3K9-modifying activities.

Jmjd2c facilitates the assembly of essential enhancer-protein complexes in ESC-derived epiblast stem cells

We observed that, similar to H3K4me1, Jmjd2c pre-marks a large panel of tissue-specific enhancers in ESCs prior to gene activation and lineage specification (Fig. 3). We therefore hypothesised that, instead of protecting regulatory regions from the acquisition of repressive marks, Jmjd2c might facilitate and/or stabilise the assembly of enhancer-associated proteins, including G9a, at the onset of differentiation. To explore this, we compared the enrichment profiles of Jmjd2c, p300, Oct4, G9a, Med1 and Smc1a in *Jmjd2c*-knockout and wild-type ESC-derived cEpiSCs by ChIP-qPCR. For this analysis, we focussed on the previously delineated *Fgf5* poised enhancer (PE) in ESCs, or on newly established (E1 and E3) enhancers produced by *Fgf5* activation in post-implantation epiblast-like cells (Fig. 6A) (Buecker et al., 2014). These sites are co-occupied by Jmjd2c and G9a, as verified in wild-type cEpiSCs (Fig. 6B, left panel).

All three *Fgf5* enhancer (PE, E1 and E3) elements examined were similarly bound by Oct4 and p300, and harboured high levels of p300-mediated H3K27ac deposition in wild-type and *Jmjd2c*-knockout cEpiSCs (Fig. 6B; data not shown). This suggests that Jmjd2c is not required for the binding of the pioneer transcription factor Oct4 and/or for the establishment of permissive chromatin at enhancers. Despite similar detection of protein levels in wild-type and knockout samples (Fig. S12A), we observed that Jmjd2c loss

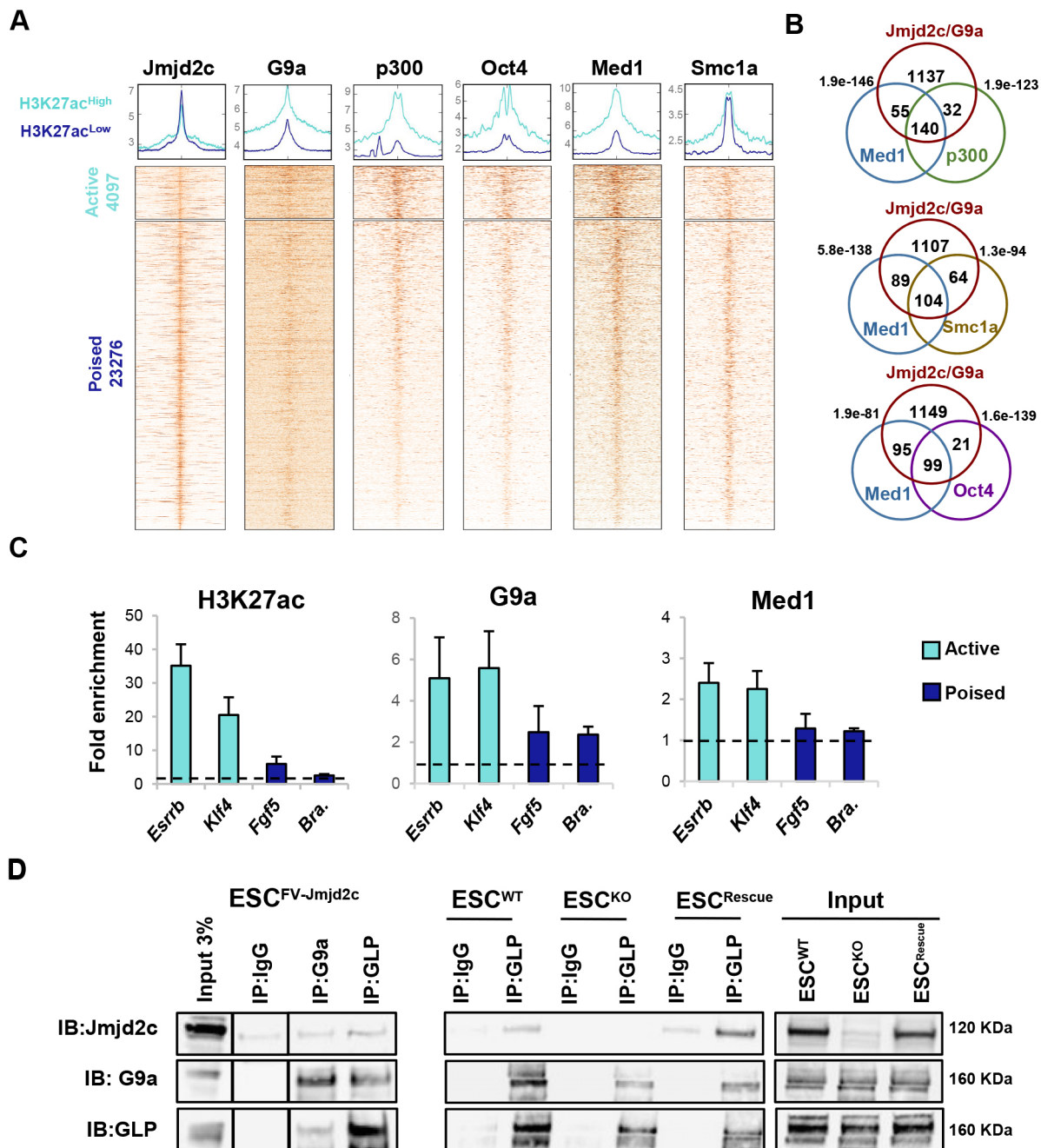


Fig. 5. Jmjd2c and G9a co-occupy active and poised enhancers in ESCs. (A) Average density plots and heatmaps showing enrichment levels for Jmjd2c, G9a, p300, Oct4, Med1 and Smc1a within a 10 kb window centred at H3K27ac-high (light blue) and H3K27ac-low (dark blue) Jmjd2c distal peaks. Scales are adjusted to maximum peak intensity for each dataset. (B) G9a peaks intersecting with Jmjd2c-distal H3K27ac-high sites are selected for this analysis. Depicted are the numbers of G9a/Jmjd2c peaks overlapping with Med1/p300, Med1/Oct4 and Med1/Smc1a (maximum gap 200 bp). *P*-values are calculated using hypergeometric tests. (C) Enrichment levels for H3K27ac, G9a and Med1 at enhancers of active (*Esrrb* and *Klf4*) and lineage-specific (*Fgf5* and brachyury) genes, as assessed by ChIP-qPCR. Data are relative to an intergenic region (dotted line) and represent mean \pm s.e.m. of three experiments. (D) (Left) G9a and GLP immunoprecipitations performed in nuclear fractions of ESCs expressing Flag-tagged Jmjd2c (FV-Jmjd2c). Input corresponds to control ESCs. Lanes were cropped and repositioned for clarity. (Middle and right panels) GLP immunoprecipitation performed in nuclear fractions of wild-type, *Jmjd2c*-KO and full-length *Jmjd2c* rescue ESCs. Interactions are visualised using immunoblotting. Data represent duplicate experiments.

abrogated G9a recruitment, as seen at the ESC stage (Fig. S11D, right panel), and furthermore destabilised the loading of the essential enhancer-associated factors Med1 and Smc1a (Fig. 6B), potentially impeding *Fgf5* expression in *Jmjd2c*-knockout cEpiSCs (Fig. S5A). Remarkably, we identified that G9a, Med1 and Smc1a binding were similarly compromised at poised enhancers of germ layer markers

(*Zic1* and brachyury) prior to gene activation (Fig. S12B). Based on these findings, we propose that inefficient assembly of activating protein complexes at poised and newly established enhancers could account for the impaired activation of lineage-affiliated genes that we have observed upon somatic differentiation in *Jmjd2c*-knockout pluripotent stem cells (Figs 1E and 2).

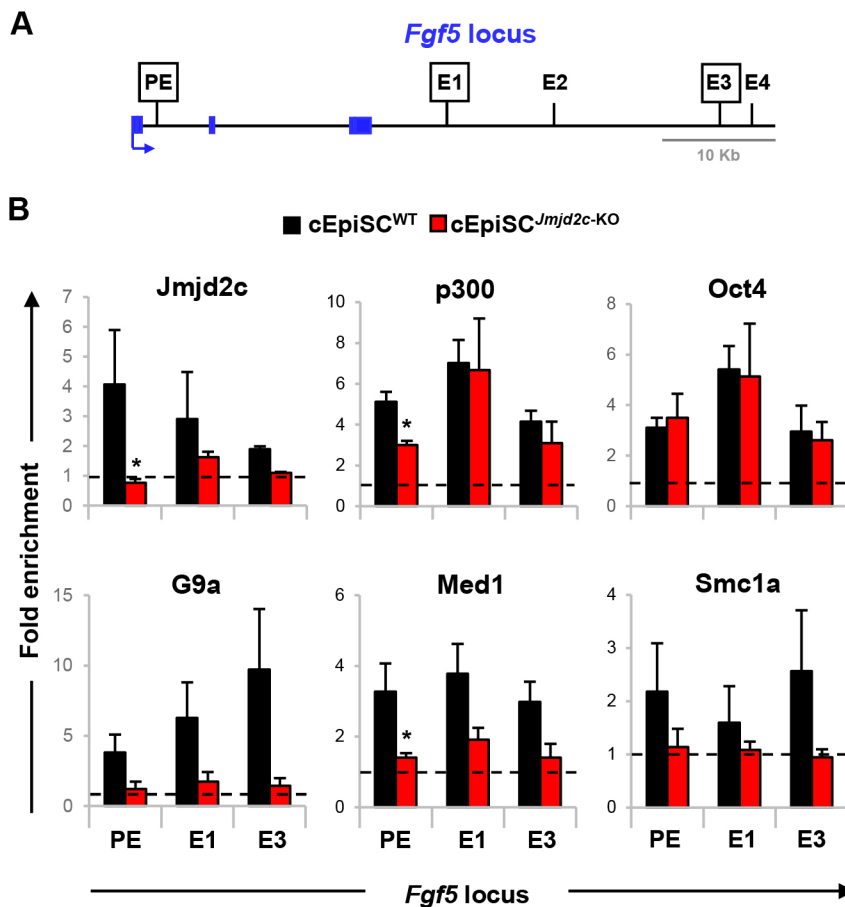


Fig. 6. Assembly of enhancer-protein complexes is destabilised in the absence of Jmjd2c in ESC-derived EpiSCs. (A) Mapping of poised (PE) and epiblast-specific enhancer sites (E1–E4) at *Fgf5* locus (Buecker et al., 2014). (B) Enrichment levels for Jmjd2c, p300, Oct4, G9a, Med1 and Smc1a at indicated sites as assessed by ChIP-qPCR in wild-type and *Jmjd2c*-KO cEpiSCs. Fold enrichment is relative to an intergenic region (dotted line) and represents mean \pm s.e.m. of three experiments. * $P < 0.05$; Mann–Whitney *U*-test.

DISCUSSION

In this study, we have identified a novel regulatory function for Jmjd2c at tissue-specific enhancers during ESC priming for differentiation. We show that Jmjd2c is required for successful multi-lineage differentiation, as assessed by EB formation. In the absence of Jmjd2c, EBs were smaller and ineffective at inducing expression of differentiation-associated genes, including early markers of the three mesoderm, endoderm and ectoderm lineages. Moreover, we established that ESC differentiation was impeded or stalled at an early post-implantation epiblast-like stage. Indeed, while *Jmjd2c*-knockout ESCs could transit into self-renewing cEpiSCs, these cells failed to establish a functionally primed state – a point that was reinforced here by their inability to further progress into mesodermal progenitors. By contrast, we found that *Jmjd2c*-knockout ESCs could readily differentiate into primitive endoderm-like derivatives under permissive conditions, as recently confirmed in triple *Jmjd2abc*-knockout models (Pedersen et al., 2016). Interestingly, however, among the three *Jmjd2* family members, *Jmjd2c* is uniquely downregulated in the primitive endoderm of the developing blastocyst, while being upregulated in the epiblast at peri-implantation times (Fig. S3) (Boroviak et al., 2015). This *in vivo* expression pattern most closely concurs with a primary role for Jmjd2c in the epiblast, while being dispensable for the formation of extra-embryonic tissues, as demonstrated in this study using ESC, EpiSC and XEN *in vitro* models.

We confirmed that *Jmjd2c* knockout is not detrimental to ESC proliferation and the maintenance of an undifferentiated phenotype upon prolonged culture (Pedersen et al., 2014), a conclusion here extended to ESC-derived EpiSCs. These results reiterate

the robustness of pluripotent stem cell self-renewal, most likely reflecting compensation mechanisms among related transcriptional regulators, including Jmjd2 family members (Pedersen et al., 2016). These results, however, contrast with earlier studies showing that shRNA-mediated *Jmjd2c* depletion led to spontaneous ESC differentiation and/or de-repression of many lineage-specific markers (Das et al., 2014; Loh et al., 2007). The discrepancies between these differing phenotypes could relate to differences in genetic backgrounds, culture conditions and the use of different knockdown constructs versus the study of constitutive knockout ESC models. Importantly, our conclusion that *Jmjd2c*-depleted ESCs self-renew normally yet fail to properly differentiate into epiblast-derived progenitors is based on concurring functional characterisation of *Jmjd2c*-knockout and -knockdown models, thus ruling out off-target effects commonly associated with shRNA approaches. Previously published studies of Jmjd2c function in ESCs (Das et al., 2014; Loh et al., 2007; Pedersen et al., 2014) did not investigate the impact of *Jmjd2c* depletion on the differentiation abilities of ESCs upon EB formation and lineage-specific induction, which precludes further comparison.

Interestingly, ectopically expressing *Jmjd2c* in ESCs also led to differentiation inhibition upon EB formation (data not shown). This finding, together with Jmjd2c being normally downregulated during this process, points to an important role for this protein at the onset of differentiation. Accordingly, we found that Jmjd2c is recruited in a timely manner to lineage-specific enhancers upon ESC priming for differentiation. By directly comparing Jmjd2c genome-wide DNA-binding sites in 2i/LIF and serum/LIF, we confirmed that Jmjd2c is prevalently bound to H3K4me3-rich TSS regions of

active and differentiation-associated genes in 2i/LIF. Strikingly, however, we identified that a significant fraction of serum/LIF-specific Jmjd2c-binding sites maps away from TSS regions, overlapping with H3K4me1/me2-rich enhancer regions in the vicinity of the same cohort of gene targets. Although Jmjd2c binding is less abundant at distal relative to TSS sites (Fig. S8 and Fig. S10), we confirmed that Jmjd2c is similarly recruited, at least in part, to enhancers and cognate promoters via its Tudor domains, most likely by recognition of H3K4me2/1 and H3K4me3, respectively (Pedersen et al., 2014). This corroborates with Jmjd2c detection in H3K4me3- and H3K4me1-coupled proteome datasets, as recently reported (Engelen et al., 2015). Given that regulatory regions nucleate the binding of numerous transcriptional regulators and co-factors, resident molecules might also contribute to Jmjd2c recruitment via protein-protein interaction at these sites.

Remarkably, however, Jmjd2c was found similarly enriched at active and pre-marked (poised) enhancers in serum/LIF (Fig. 5), suggesting that Jmjd2c could act as a molecular platform for the recruitment of enhancer constituents. In particular, we asked whether the loss of Jmjd2c in ESCs might impact on Oct4 and p300 re-distribution at newly activated (*Fgf5*) enhancer sites upon ESC-to-EpiSC conversion. Binding of Oct4, p300 and p300-mediated H3K27ac deposition were, however, retained at *Fgf5* in *Jmjd2c*-knockout cEpiSCs. Instead, we established that Jmjd2c was required for the proper binding of Med1 and Smc1a at active (*Fgf5*) and poised enhancers in epiblast-like cells (Fig. 6 and Fig. S12). A facilitating role for Jmjd2c in the assembly of activating enhancer-protein complexes was also supported by the ability of Jmjd2c to physically interact with G9a and Med1 in ESCs. Together, these findings suggest that, in the absence of Jmjd2c, inefficient loading of essential mediator-cohesin complexes at lineage-specific enhancers impairs the activation of affiliated genes, accounting for the differentiation defect observed in *Jmjd2c*-knockout cells.

Given the established role of mediator and cohesin in bridging enhancers and core promoters (Kagey et al., 2010), we speculate that Jmjd2c recruitment to enhancers might coincide and/or contribute to DNA looping events prior to gene activation and lineage specification (Fig. 7). In line with this model, we find that Jmjd2c-bound distal peaks closely align with promoter-enhancer interaction sites, as shown in the vicinity of *Foxa2* in ESCs (Fig. S13). Interestingly, we note that the stability of all Jmjd2c-bound promoter-enhancer interactions observed across the genome is significantly enhanced in serum/LIF when compared with 2i/LIF (CHiCAGO score analysis, P -value 2.446×10^{-12} ; O.J. and H.G.S., unpublished), correlating with Jmjd2c re-distribution to poised enhancers during ESC priming for differentiation. However, and given that ChIP and Hi-C approaches commonly employ crosslinked chromatin, it remains unclear whether the increased detection of Jmjd2c at enhancers might be the cause or the result of stabilised promoter-enhancer interactions in serum/LIF.

An intriguing finding arising from this study is the co-recruitment of the H3K9-methyltransferase G9a to Jmjd2c-bound distal peaks in ESCs. Contrasting with its canonical role in gene silencing (Feldman et al., 2006; Mozzetta et al., 2014), highest G9a co-enrichment levels were unexpectedly observed at ESC-specific, Jmjd2c-bound enhancers, suggesting that G9a/Jmjd2c co-enrichment might coincide with the formation of activating complexes. Moreover, and similar to Oct4, p300, Med1 and Smc1a, G9a was also present at lineage-specific, Jmjd2c-bound enhancers, although at reduced levels in ESCs. In the absence of Jmjd2c, G9a binding was destabilised, as also demonstrated in ESC-derived cEpiSCs along with Med1 and Smc1a. Interestingly, G9a was found to be capable of interacting with Jmjd2c, Med1 or CDYL, suggesting that G9a can form both activating and repressive complexes in ESCs (Fritsch et al., 2010). This is in agreement with previous reports showing that G9a is co-recruited and interacts with either the co-activator Med1 or the co-repressor Jarid1 in a mutually exclusive manner at β -globin genes during haematopoiesis (Chaturvedi et al., 2012; Shankar et al., 2013). Remarkably, and consistent with a dual role for G9a in regulating gene expression, we find that Jmjd2c-G9a co-bound targets are significantly enriched among differentially expressed genes in *G9a*-knockout ESCs (Mozzetta et al., 2014) and E8.5 embryos (Auclair et al., 2016), showing clear evidence for both gene upregulation and downregulation *in vitro* and *in vivo* (Fig. S14). Notably, genes associated with developmental processes are prevalently downregulated in E8.5 embryos in the absence of G9a as previously documented (Auclair et al., 2016; Mozzetta et al., 2014). However, the mechanisms underlying the action of G9a as repressor and activator in ESCs and in other cellular contexts (Chaturvedi et al., 2012; Shankar et al., 2013) remain unknown.

Despite a global increase in H3K9me2 levels in the absence of Jmjd2c, we did not detect any aberrant acquisition of H3K9 and DNA methylation at Jmjd2c/G9a co-bound lineage-affiliated genes in *Jmjd2c*-knockout ESCs, in cEpiSCs or upon lineage specification (Fig. 4; data not shown). This argued against a role for Jmjd2c in continually removing G9a-mediated H3K9me2 deposition, implying novel histone-independent roles for Jmjd2c and G9a at tissue-specific enhancers. Although the precise molecular interplays between the two molecules need to be fully deciphered, we note that G9a automethylation sites, which anchor the binding of repressive complexes (Ruan et al., 2012), were previously identified as potential targets for Jmjd2c-mediated demethylation (Ponnaluri et al., 2009). Whether demethylation of G9a by Jmjd2c via its catalytic domain is a prerequisite for interaction with activating complexes needs to be studied. More generally, further elucidating how Jmjd2c and other histone demethylases might act as key post-translational regulators to promote the assembly of activating enhancer-protein complexes could indeed provide novel important insights into the regulation of enhancer activity and gene expression in stem cells and development.

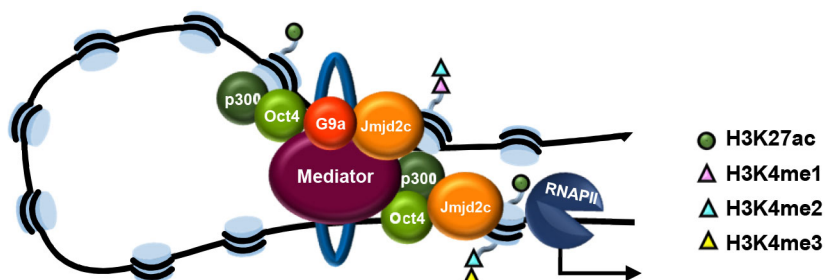


Fig. 7. Proposed model: assembly of activating Jmjd2c-G9a centred enhancer-protein complexes. Jmjd2c and G9a co-occupy poised (lineage-specific) enhancers in primed ESCs where they stabilise the assembly of mediator-cohesin complexes (Kagey et al., 2010) that are necessary for the formation of DNA loops and for potent gene activation at the exit of pluripotency and upon differentiation.

MATERIALS AND METHODS

Cell culture

Mouse ESCs were cultured as previously described (Alder et al., 2010) with 10% FBS (serum), LIF or adapted to serum-free conditions (N2B27 with 1 μ M PD0325901, 3 μ M CHIR99021 and LIF), as described previously (Ying et al., 2008). Generation of ESC lines are described in the supplementary Materials and Methods, and primers used for genotyping/cloning are listed in Tables S2 and S3.

ESC differentiation was induced in embryoid bodies (EBs) (ultra-low attachment plates, Corning, in 5% FBS without LIF) or with addition of 1 μ M all-trans retinoic-acid (atRA) in 5% FBS without LIF. For mesoderm differentiation, EpiSCs were cultured in FLYB media (bFGF, LY294002 and BMP4) for 36 h followed by either FB40 (bFGF and BMP4) or FLYWLDN (bFGF, LY294002, Wnt3a and LDN193189) media as previously described (Cheung et al., 2012). Full media composition and generation of cEpiSCs are outlined in the supplementary Materials and Methods.

Quantitative PCR

RNA was isolated with the RNeasy mini kit (Qiagen) and reverse-transcribed using SuperScript II (Invitrogen). cDNA/DNA was amplified with KicQstart SYBR Green PCR Mastermix (Sigma). Details and primer sequences are listed in the supplementary Materials and Methods and Table S4.

Immunofluorescence staining

Cells fixed with 4% paraformaldehyde were permeabilised/blocked for 30 min in 0.4% TritonX-100 and 10% serum. Primary antibody (see Table S1) incubation occurred overnight at 4°C. Fluorophore-conjugated secondary antibodies (ThermoFisher) were incubated for 1 h. Fluorescence was visualised on a SP5 Leica confocal microscope or a fluorescent/brightfield microscope. For further details, see supplementary Materials and Methods.

Flow cytometry analysis

Cells were harvested using cell dissociation buffer (Gibco), blocked in 2% FBS and analysed on an Accuri C6 Flow cytometer. For details on the antibodies used, see supplementary Materials and Methods.

RNA-seq analysis

Computational analysis on previously published RNA-seq datasets generated in G9a-knockout and wild-type embryos and ESCs are described in the supplementary Materials and Methods.

Immunoblotting, immunoprecipitation, ChIP and ChIP-seq

Whole-cell lysates and acid-extracted histones (Shechter et al., 2007) were resolved on SDS-PAGE gels and transferred into PVDF membranes (GE Healthcare). Immunoprecipitation and chromatin immunoprecipitation (ChIP) were performed as previously described (Battisti et al., 2016; Frank et al., 2001; Fritsch et al., 2010). Experimental details and information about computational analysis are outlined in the supplementary Materials and Methods. Primers used for the ChIP can be found in Tables S5 and S6.

Acknowledgements

We are grateful to Huck-Hui Ng for antibodies and shRNA vectors; to William Skarnes, Jennifer Nichols, Roger Pedersen and Janet Rossant for cell lines; to Raymond Poot and Ian Chambers for plasmids; to Ludovic Vallier for reagents; and to Fabrice Laval, Sergio German, Anne Helness, Julien Pontis, Van Nguyen, Vincent Brochard and Shuangyin Wang for their technical and bioinformatics assistance. We thank the Advanced Sequencing Facility at the Francis Crick Institute and Wei Cui, Alice Jouneau and Tristan Rodriguez for discussions and/or critical reading of the manuscript.

Competing interests

The authors declare no competing or financial interests.

Author contributions

R.A.T. conducted most of the experiments; J.L.H. and H.F.J. performed mesoderm differentiations; D.K. and L.W. conducted knockdown and rescue experiments; L.F.

and S.A.-S.-A. conducted co-immunoprecipitation experiments and advised on G9a ChIP; T.B.-K. performed anti-Flag ChIP; E.B. and E.C. analysed ChIP/RNA-seq datasets; I.d.V.T. and K.K.N. assisted on bioinformatics and ESC-to-XEN cell conversion; C.F. generated *Jmjd2c*-knockout ESCs; O.J. and H.G.S. performed ChIPAGO analyses on unpublished Hi-C capture datasets; R.A.T. and V.A. prepared the manuscript; V.A. conceived the project.

Funding

This work was supported by the Fundação para a Ciência e a Tecnologia (Portugal) (SFRH/BD/70242/2010), by the Genesis Research Trust (P55000), by the British Heart Foundation (PG/12/86/29930), by an Imperial College London President's PhD Scholarship (STU0082882), by the Centre National de la Recherche Scientifique, by the Medical Research Council (MR/K00090X/1 and MR/K500793/1), by the Wellcome Trust Sanger Institute, by the Francis Crick Institute [which receives its core funding from Cancer Research UK (FC001120), the UK Medical Research Council (FC001120) and the Wellcome Trust (FC001120)], by a European Research Council grant (ERC-2013-ADG, 339431 'SysStemCell') and by Imperial College London. Deposited in PMC for immediate release.

Data availability

ChIP-seq data has been deposited into Gene Expression Omnibus under the accession number GSE93721.

Supplementary information

Supplementary information available online at <http://dev.biologists.org/lookup/doi/10.1242/dev.142489.supplemental>

References

- Alder, O., Laval, F., Helness, A., Brookes, E., Pinho, S., Chandrasekharan, A., Arnaud, P., Pombo, A., O'Neill, L. and Azuara, V. (2010). Ring1B and Suv39h1 delineate distinct chromatin states at bivalent genes during early mouse lineage commitment. *Development* **137**, 2483–2492.
- Artus, J., Panthier, J.-J. and Hadjantonakis, A.-K. (2010). A role for PDGF signaling in expansion of the extra-embryonic endoderm lineage of the mouse blastocyst. *Development* **137**, 3361–3372.
- Artus, J., Douvaras, P., Piliszek, A., Isern, J., Baron, M. H. and Hadjantonakis, A.-K. (2012). BMP4 signaling directs primitive endoderm-derived XEN cells to an extraembryonic visceral endoderm identity. *Dev. Biol.* **361**, 245–262.
- Auclair, G., Borgel, J., Sanz, L. A., Vallet, J., Guibert, S., Dumas, M., Cavelier, P., Girardot, M., Forné, T., Feil, R. et al. (2016). EHMT2 directs DNA methylation for efficient gene silencing in mouse embryos. *Genome Res.* **26**, 192–202.
- Azuara, V., Perry, P., Sauer, S., Spivakov, M., Jørgensen, H. F., John, R. M., Gouti, M., Casanova, M., Warnes, G., Merkschlager, M. et al. (2006). Chromatin signatures of pluripotent cell lines. *Nat. Cell Biol.* **8**, 532–538.
- Battisti, V., Pontis, J., Boyarchuk, E., Fritsch, L., Robin, P., Ait-Si-Ali, S. and Joliet, V. (2016). Unexpected distinct roles of the related histone H3 lysine 9 methyltransferases G9a and G9a-like protein in myoblasts. *J. Mol. Biol.* **428**, 2329–2343.
- Bernstein, B. E., Mikkelsen, T. S., Xie, X., Kamal, M., Huebert, D. J., Cuff, J., Fry, B., Meissner, A., Wernig, M., Plath, K. et al. (2006). A bivalent chromatin structure marks key developmental genes in embryonic stem cells. *Cell* **125**, 315–326.
- Boroviak, T. and Nichols, J. (2014). The birth of embryonic pluripotency. *Philos. Trans. R. Soc. Lond. B Biol. Sci.* **369**, pii 20130541.
- Boroviak, T., Loos, R., Lombard, P., Okahara, J., Behr, R., Sasaki, E., Nichols, J., Smith, A. and Bertone, P. (2015). Lineage-specific profiling delineates the emergence and progression of naive pluripotency in mammalian embryogenesis. *Dev. Cell* **35**, 366–382.
- Bradley, A., Anastassiadis, K., Ayadi, A., Battey, J. F., Bell, C., Birling, M.-C., Bottomley, J., Brown, S. D., Bürger, A., Bult, C. J. et al. (2012). The mammalian gene function resource: the International Knockout Mouse Consortium. *Mamm. Genome* **23**, 580–586.
- Brons, I. G. M., Smithers, L. E., Trotter, M. W. B., Rugg-Gunn, P., Sun, B., Chuva de Sousa Lopes, S. M., Howlett, S. K., Clarkson, A., Ahrlund-Richter, L., Pedersen, R. A. et al. (2007). Derivation of pluripotent epiblast stem cells from mammalian embryos. *Nature* **448**, 191–195.
- Buecker, C., Srinivasan, R., Wu, Z., Calo, E., Acampora, D., Faial, T., Simeone, A., Tan, M., Swigut, T. and Wysocka, J. (2014). Reorganization of enhancer patterns in transition from naive to primed pluripotency. *Cell Stem Cell* **14**, 838–853.
- Burton, A., Muller, J., Tu, S., Padilla-Longoria, P., Guccione, E. and Torres-Padilla, M.-E. (2013). Single-cell profiling of epigenetic modifiers identifies PRDM14 as an inducer of cell fate in the mammalian embryo. *Cell Rep.* **5**, 687–701.
- Calo, E. and Wysocka, J. (2013). Modification of enhancer chromatin: what, how, and why? *Mol. Cell* **49**, 825–837.

- Capo-Chichi, C. D., Rula, M. E., Smedberg, J. L., Vanderveer, L., Parmacek, M. S., Morrissey, E. E., Godwin, A. K. and Xu, X.-X. (2005). Perception of differentiation cues by GATA factors in primitive endoderm lineage determination of mouse embryonic stem cells. *Dev. Biol.* **286**, 574–586.
- Chaturvedi, C.-P., Somasundaram, B., Singh, K., Carpenedo, R. L., Stanford, W. L., Dilworth, F. J. and Brand, M. (2012). Maintenance of gene silencing by the coordinate action of the H3K9 methyltransferase G9a/KMT1C and the H3K4 demethylase Jarid1a/KDM5A. *Proc. Natl. Acad. Sci. USA* **109**, 18845–18850.
- Chen, T. and Dent, S. Y. R. (2014). Chromatin modifiers and remodellers: regulators of cellular differentiation. *Nat. Rev. Genet.* **15**, 93–106.
- Chen, Z., Zang, J., Whetstone, J., Hong, X., Davrazou, F., Kutateladze, T. G., Simpson, M., Mao, Q., Pan, C.-H., Dai, S. et al. (2006). Structural insights into histone demethylation by JMJD2 family members. *Cell* **125**, 691–702.
- Cheung, C., Bernardo, A. S., Trotter, M. W. B., Pedersen, R. A. and Sinha, S. (2012). Generation of human vascular smooth muscle subtypes provides insight into embryological origin-dependent disease susceptibility. *Nat. Biotechnol.* **30**, 165–173.
- Cho, L. T. Y., Wamaitha, S. E., Tsai, I. J., Artus, J., Sherwood, R. I., Pedersen, R. A., Hadjantonakis, A.-K. and Niakan, K. K. (2012). Conversion from mouse embryonic to extra-embryonic endoderm stem cells reveals distinct differentiation capacities of pluripotent stem cell states. *Development* **139**, 2866–2877.
- Chung, Y., Klimanskaya, I., Becker, S., Marh, J., Lu, S.-J., Johnson, J., Meisner, L. and Lanza, R. (2006). Embryonic and extraembryonic stem cell lines derived from single mouse blastomeres. *Nature* **439**, 216–219.
- Cloos, P. A. C., Christensen, J., Agger, K., Maiolica, A., Rappsilber, J., Antal, T., Hansen, K. H. and Helin, K. (2006). The putative oncogene GASC1 demethylates tri- and dimethylated lysine 9 on histone H3. *Nature* **442**, 307–311.
- Creyghton, M. P., Cheng, A. W., Welstead, G. G., Kooistra, T., Carey, B. W., Steine, E. J., Hanna, J., Lodato, M. A., Frampton, G. M., Sharp, P. A. et al. (2010). Histone H3K27ac separates active from poised enhancers and predicts developmental state. *Proc. Natl. Acad. Sci. USA* **107**, 21931–21936.
- Das, P. P., Shao, Z., Beyaz, S., Apostolou, E., Pinello, L., De Los Angeles, A., O'Brien, K., Atsma, J. M., Fujiwara, Y., Nguyen, M. et al. (2014). Distinct and combinatorial functions of Jmjd2b/Kdm4b and Jmjd2c/Kdm4c in mouse embryonic stem cell identity. *Mol. Cell* **53**, 32–48.
- Deaton, A. M. and Bird, A. (2011). CpG islands and the regulation of transcription. *Genes Dev.* **25**, 1010–1022.
- Efroni, S., Duttagupta, R., Cheng, J., Dehghani, H., Hoepfner, D. J., Dash, C., Bazett-Jones, D. P., Le Grice, S., McKay, R. D. G., Buetow, K. H. et al. (2008). Global transcription in pluripotent embryonic stem cells. *Cell Stem Cell* **2**, 437–447.
- Engelen, E., Brandsma, J. H., Moen, M. J., Signorile, L., Dekkers, D. H. W., Demmers, J., Kockx, C. E. M., Ozgür, Z., van Ijcken, W. F. J., van den Berg, D. L. C. et al. (2015). Proteins that bind regulatory regions identified by histone modification chromatin immunoprecipitations and mass spectrometry. *Nat. Commun.* **6**, 7155.
- Evans, M. J. and Kaufman, M. H. (1981). Establishment in culture of pluripotential cells from mouse embryos. *Nature* **292**, 154–156.
- Farcas, A. M., Blackledge, N. P., Sudbery, I., Long, H. K., McGouran, J. F., Rose, N. R., Lee, S., Sims, D., Cerase, A., Sheahan, T. W. et al. (2012). KDM2B links the Polycomb Repressive Complex 1 (PRC1) to recognition of CpG islands. *Elife* **1**, e00205.
- Feldman, N., Gerson, A., Fang, J., Li, E., Zhang, Y., Shinkai, Y., Cedar, H. and Bergman, Y. (2006). G9a-mediated irreversible epigenetic inactivation of Oct-3/4 during early embryogenesis. *Nat. Cell Biol.* **8**, 188–194.
- Frank, S. R., Schroeder, M., Fernandez, P., Taubert, S. and Amati, B. (2001). Binding of c-Myc to chromatin mediates mitogen-induced acetylation of histone H4 and gene activation. *Genes Dev.* **15**, 2069–2082.
- Fritsch, L., Robin, P., Mathieu, J. R. R., Souidi, M., Hinaux, H., Rougeulle, C., Harel-Bellan, A., Ameyar-Zazoua, M. and Ait-Si-Ali, S. (2010). A subset of the histone H3 lysine 9 methyltransferases Suv39h1, G9a, GLP, and SETDB1 participate in a multimeric complex. *Mol. Cell* **37**, 46–56.
- Gibcus, J. H. and Dekker, J. (2013). The hierarchy of the 3D genome. *Mol. Cell* **49**, 773–782.
- Guo, G., Yang, J., Nichols, J., Hall, J. S., Eyres, I., Mansfield, W. and Smith, A. (2009). Klf4 reverts developmentally programmed restriction of ground state pluripotency. *Development* **136**, 1063–1069.
- Heinz, S., Benner, C., Spann, N., Bertolino, E., Lin, Y. C., Laslo, P., Cheng, J. X., Murre, C., Singh, H. and Glass, C. K. (2010). Simple combinations of lineage-determining transcription factors prime cis-regulatory elements required for macrophage and B cell identities. *Mol. Cell* **38**, 576–589.
- Hon, G. C., Song, C.-X., Du, T., Jin, F., Selvaraj, S., Lee, A. Y., Yen, C.-A., Ye, Z., Mao, S.-Q., Wang, B.-A. et al. (2014). 5mC oxidation by Tet2 modulates enhancer activity and timing of transcriptome reprogramming during differentiation. *Mol. Cell* **56**, 286–297.
- Illingworth, R. S. and Bird, A. P. (2009). CpG islands—'a rough guide'. *FEBS Lett.* **583**, 1713–1720.
- Kagey, M. H., Newman, J. J., Bilodeau, S., Zhan, Y., Orlando, D. A., van Berkum, N. L., Ebmeier, C. C., Goossens, J., Rahl, P. B., Levine, S. S. et al. (2010). Mediator and cohesin connect gene expression and chromatin architecture. *Nature* **467**, 430–435.
- Klose, R. J., Yamane, K., Bae, Y., Zhang, D., Erdjument-Bromage, H., Tempst, P., Wong, J. and Zhang, Y. (2006). The transcriptional repressor JHDM3A demethylates trimethyl histone H3 lysine 9 and lysine 36. *Nature* **442**, 312–316.
- Kunath, T., Arnaud, D., Uy, G. D., Okamoto, I., Chureau, C., Yamanaka, Y., Heard, E., Gardner, R. L., Avner, P. and Rossant, J. (2005). Imprinted X-inactivation in extra-embryonic endoderm cell lines from mouse blastocysts. *Development* **132**, 1649–1661.
- Langmead, B. and Salzberg, S. L. (2012). Fast gapped-read alignment with Bowtie 2. *Nat. Methods* **9**, 357–359.
- Lienert, F., Mohn, F., Tiwari, V. K., Baubec, T., Roloff, T. C., Gaidatzis, D., Stadler, M. B. and Schübeler, D. (2011). Genomic prevalence of heterochromatic H3K9me2 and transcription do not discriminate pluripotent from terminally differentiated cells. *PLoS Genet.* **7**, e1002090.
- Liu, N., Zhang, Z., Wu, H., Jiang, Y., Meng, L., Xiong, J., Zhao, Z., Zhou, X., Li, J., Li, H. et al. (2015). Recognition of H3K9 methylation by GLP is required for efficient establishment of H3K9 methylation, rapid target gene repression, and mouse viability. *Genes Dev.* **29**, 379–393.
- Loh, Y.-H., Zhang, W., Chen, X., George, J. and Ng, H.-H. (2007). Jmjd1a and Jmjd2c histone H3 Lys 9 demethylases regulate self-renewal in embryonic stem cells. *Genes Dev.* **21**, 2545–2557.
- Marks, H., Kalkan, T., Menafra, R., Denissov, S., Jones, K., Hofmeister, H., Nichols, J., Kranz, A., Stewart, A. F., Smith, A. et al. (2012). The transcriptional and epigenomic foundations of ground state pluripotency. *Cell* **149**, 590–604.
- Marson, A., Levine, S. S., Cole, M. F., Frampton, G. M., Brambrink, T., Johnstone, S., Guenther, M. G., Johnston, W. K., Wernig, M., Newman, J. et al. (2008). Connecting microRNA genes to the core transcriptional regulatory circuitry of embryonic stem cells. *Cell* **134**, 521–533.
- Martin, G. R. (1981). Isolation of a pluripotent cell line from early mouse embryos cultured in medium conditioned by teratocarcinoma stem cells. *Proc. Natl. Acad. Sci. USA* **78**, 7634–7638.
- Mozzetta, C., Pontis, J., Fritsch, L., Robin, P., Portoso, M., Proux, C., Margueron, R. and Ait-Si-Ali, S. (2014). The histone H3 lysine 9 methyltransferases G9a and GLP regulate polycomb repressive complex 2-mediated gene silencing. *Mol. Cell* **53**, 277–289.
- Ng, H.-H. and Surani, M. A. (2011). The transcriptional and signalling networks of pluripotency. *Nat. Cell Biol.* **13**, 490–496.
- Niakan, K. K., Schrodde, N., Cho, L. T. Y. and Hadjantonakis, A.-K. (2013). Derivation of extraembryonic endoderm stem (XEN) cells from mouse embryos and embryonic stem cells. *Nat. Protoc.* **8**, 1028–1041.
- Nichols, J. and Smith, A. (2009). Naive and primed pluripotent states. *Cell Stem Cell* **4**, 487–492.
- Niwa, H., Burdon, T., Chambers, I. and Smith, A. (1998). Self-renewal of pluripotent embryonic stem cells is mediated via activation of STAT3. *Genes Dev.* **12**, 2048–2060.
- Nottke, A., Colaiacovo, M. P. and Shi, Y. (2009). Developmental roles of the histone lysine demethylases. *Development* **136**, 879–889.
- Nowak, D. E., Tian, B. and Brasier, A. R. (2005). Two-step cross-linking method for identification of NF- κ B gene network by chromatin immunoprecipitation. *Biotechniques* **39**, 715–725.
- Osorno, R., Tsakiridis, A., Wong, F., Cambray, N., Economou, C., Wilkie, R., Blin, G., Scotting, P. J., Chambers, I. and Wilson, V. (2012). The developmental dismantling of pluripotency is reversed by ectopic Oct4 expression. *Development* **139**, 2288–2298.
- Paca, A., Séguin, C. A., Clements, M., Ryczko, M., Rossant, J., Rodriguez, T. A. and Kunath, T. (2012). BMP signaling induces visceral endoderm differentiation of XEN cells and parietal endoderm. *Dev. Biol.* **361**, 90–102.
- Pedersen, M. T., Agger, K., Laugesen, A., Johansen, J. V., Cloos, P. A. C., Christensen, J. and Helin, K. (2014). The demethylase JMJD2C localizes to H3K4me3-positive transcription start sites and is dispensable for embryonic development. *Mol. Cell Biol.* **34**, 1031–1045.
- Pedersen, M. T., Kooistra, S. M., Radziszewska, A., Laugesen, A., Johansen, J. V., Hayward, D. G., Nilsson, J., Agger, K. and Helin, K. (2016). Continual removal of H3K9 promoter methylation by Jmjd2 demethylases is vital for ESC self-renewal and early development. *EMBO J.* **35**, 1483–1595.
- Ponnaluri, V. K. C., Vavilala, D. T., Putty, S., Gutheil, W. G. and Mukherji, M. (2009). Identification of non-histone substrates for JMJD2A-C histone demethylases. *Biochem. Biophys. Res. Commun.* **390**, 280–284.
- Ramirez, F., Dundar, F., Diehl, S., Gruning, B. A. and Manke, T. (2014). deepTools: a flexible platform for exploring deep-sequencing data. *Nucleic Acids Res.* **42**, W187–W191.
- Robinson, J. T., Thorvaldsdóttir, H., Winckler, W., Guttman, M., Lander, E. S., Getz, G. and Mesirov, J. P. (2011). Integrative genomics viewer. *Nat. Biotechnol.* **29**, 24–26.
- Rossant, J. (2008). Stem cells and early lineage development. *Cell* **132**, 527–531.
- Ruan, J., Ouyang, H., Amaya, M. F., Ravichandran, M., Loppnau, P., Min, J. and Zang, J. (2012). Structural basis of the chromodomain of Cbx3 bound to methylated peptides from histone h1 and G9a. *PLoS ONE* **7**, e35376.

- Senner, C. E., Krueger, F., Oxley, D., Andrews, S. and Hemberger, M. (2012). DNA methylation profiles define stem cell identity and reveal a tight embryonic-extraembryonic lineage boundary. *Stem Cells* **30**, 2732-2745.
- Shankar, S. R., Bahirvani, A. G., Rao, V. K., Bharathy, N., Ow, J. R. and Taneja, R. (2013). G9a, a multipotent regulator of gene expression. *Epigenetics* **8**, 16-22.
- Shechter, D., Dormann, H. L., Allis, C. D. and Hake, S. B. (2007). Extraction, purification and analysis of histones. *Nat. Protoc.* **2**, 1445-1457.
- Shpargel, K. B., Sengoku, T., Yokoyama, S. and Magnuson, T. (2012). UTX and UTY demonstrate histone demethylase-independent function in mouse embryonic development. *PLoS Genet.* **8**, e1002964.
- Skarnes, W. C., Rosen, B., West, A. P., Koutsourakis, M., Bushell, W., Iyer, V., Mujica, A. O., Thomas, M., Harrow, J., Cox, T. et al. (2011). A conditional knockout resource for the genome-wide study of mouse gene function. *Nature* **474**, 337-342.
- Spitz, F. and Furlong, E. E. M. (2012). Transcription factors: from enhancer binding to developmental control. *Nat. Rev. Genet.* **13**, 613-626.
- Stock, J. K., Giadrossi, S., Casanova, M., Brookes, E., Vidal, M., Koseki, H., Brockdorff, N., Fisher, A. G. and Pombo, A. (2007). Ring1-mediated ubiquitination of H2A restrains poised RNA polymerase II at bivalent genes in mouse ES cells. *Nat. Cell Biol.* **9**, 1428-1435.
- Tesar, P. J. (2005). Derivation of germ-line-competent embryonic stem cell lines from preblastocyst mouse embryos. *Proc. Natl. Acad. Sci. USA* **102**, 8239-8244.
- Tesar, P. J., Chenoweth, J. G., Brook, F. A., Davies, T. J., Evans, E. P., Mack, D. L., Gardner, R. L. and McKay, R. D. G. (2007). New cell lines from mouse epiblast share defining features with human embryonic stem cells. *Nature* **448**, 196-199.
- Torres-Padilla, M.-E. and Chambers, I. (2014). Transcription factor heterogeneity in pluripotent stem cells: a stochastic advantage. *Development* **141**, 2173-2181.
- Veillard, A.-C., Marks, H., Bernardo, A. S., Jouneau, L., Laloë, D., Boulanger, L., Kaan, A., Brochard, V., Tosolini, M., Pedersen, R. et al. (2014). Stable methylation at promoters distinguishes epiblast stem cells from embryonic stem cells and the in vivo epiblasts. *Stem Cells Dev.* **23**, 2014-2029.
- Wang, J., Zhang, M., Zhang, Y., Kou, Z., Han, Z., Chen, D.-Y., Sun, Q.-Y. and Gao, S. (2010). The histone demethylase JMJD2C is stage-specifically expressed in preimplantation mouse embryos and is required for embryonic development. *Biol. Reprod.* **82**, 105-111.
- Wang, C., Lee, J.-E., Cho, Y.-W., Xiao, Y., Jin, Q., Liu, C. and Ge, K. (2012). UTX regulates mesoderm differentiation of embryonic stem cells independent of H3K27 demethylase activity. *Proc. Natl. Acad. Sci. USA* **109**, 15324-15329.
- Whetstone, J. R., Nottke, A., Lan, F., Huarte, M., Smolikov, S., Chen, Z., Spooner, E., Li, E., Zhang, G., Colaiacovo, M. et al. (2006). Reversal of histone lysine trimethylation by the JMJD2 family of histone demethylases. *Cell* **125**, 467-481.
- Wu, X., Johansen, J. V. and Helin, K. (2013). Fbxl10/Kdm2b recruits polycomb repressive complex 1 to CpG islands and regulates H2A ubiquitylation. *Mol. Cell* **49**, 1134-1146.
- Yang, Z., Jiang, J., Stewart, D. M., Qi, S., Yamane, K., Li, J., Zhang, Y. and Wong, J. (2010). AOF1 is a histone H3K4 demethylase possessing demethylase activity-independent repression function. *Cell Res.* **20**, 276-287.
- Ying, Q.-L., Nichols, J., Chambers, I. and Smith, A. (2003). BMP induction of Id proteins suppresses differentiation and sustains embryonic stem cell self-renewal in collaboration with STAT3. *Cell* **115**, 281-292.
- Ying, Q.-L., Wray, J., Nichols, J., Battle-Morera, L., Doble, B., Woodgett, J., Cohen, P. and Smith, A. (2008). The ground state of embryonic stem cell self-renewal. *Nature* **453**, 519-523.
- Zentner, G. E., Tesar, P. J. and Scacheri, P. C. (2011). Epigenetic signatures distinguish multiple classes of enhancers with distinct cellular functions. *Genome Res.* **21**, 1273-1283.
- Zhu, L. J., Gazin, C., Lawson, N. D., Pagès, H., Lin, S. M., Lapointe, D. S. and Green, M. R. (2010). ChIPpeakAnno: a Bioconductor package to annotate ChIP-seq and ChIP-chip data. *BMC Bioinformatics* **11**, 237.

Jmjd2c/Kdm4c facilitates the assembly of essential enhancer-protein complexes at the onset of embryonic stem cell differentiation

Rute A. Tomaz, Jennifer L. Harman, Donja Karimlou, Lauren Weavers, Lauriane Fritsch, Tony Bou-Kheir, Emma Bell, Ignacio del Valle Torres, Kathy K. Niakan, Cynthia Fisher, Onkar Joshi, Hendrik G. Stunnenberg, Edward Curry, Slimane Ait-Si-Ali, Helle F. Jørgensen and Véronique Azuara

List of Supplementary Material

Figure S1 (related to Figure 1)

Figure S2 (related to Figure 1)

Figure S3 (related to Figure 1)

Figure S4 (related to Figure 1)

Figure S5 (related to Figure 2)

Figure S6 (related to Figure 2)

Figure S7 (related to Figure 3)

Figure S8 (related to Figure 3)

Figure S9 (related to Figure 4)

Figure S10 (related to Figure 5)

Figure S11 (related to Figure 5)

Figure S12 (related to Figure 6)

Figure S13 (related to Figure 7)

Figure S14 (related to Figure 7)

Table S1 (antibodies used in this study)

Table S2 (sequences of primers used for genotyping)

Table S3 (sequences of primers used for cloning)

Table S4 (sequences of primers used for RT-qPCR)

Table S5 (sequences of primers used for ChIP)

Table S6 (sequences of primers used for H3K9me2 ChIP)

Supplementary Materials and Methods

Supplementary References

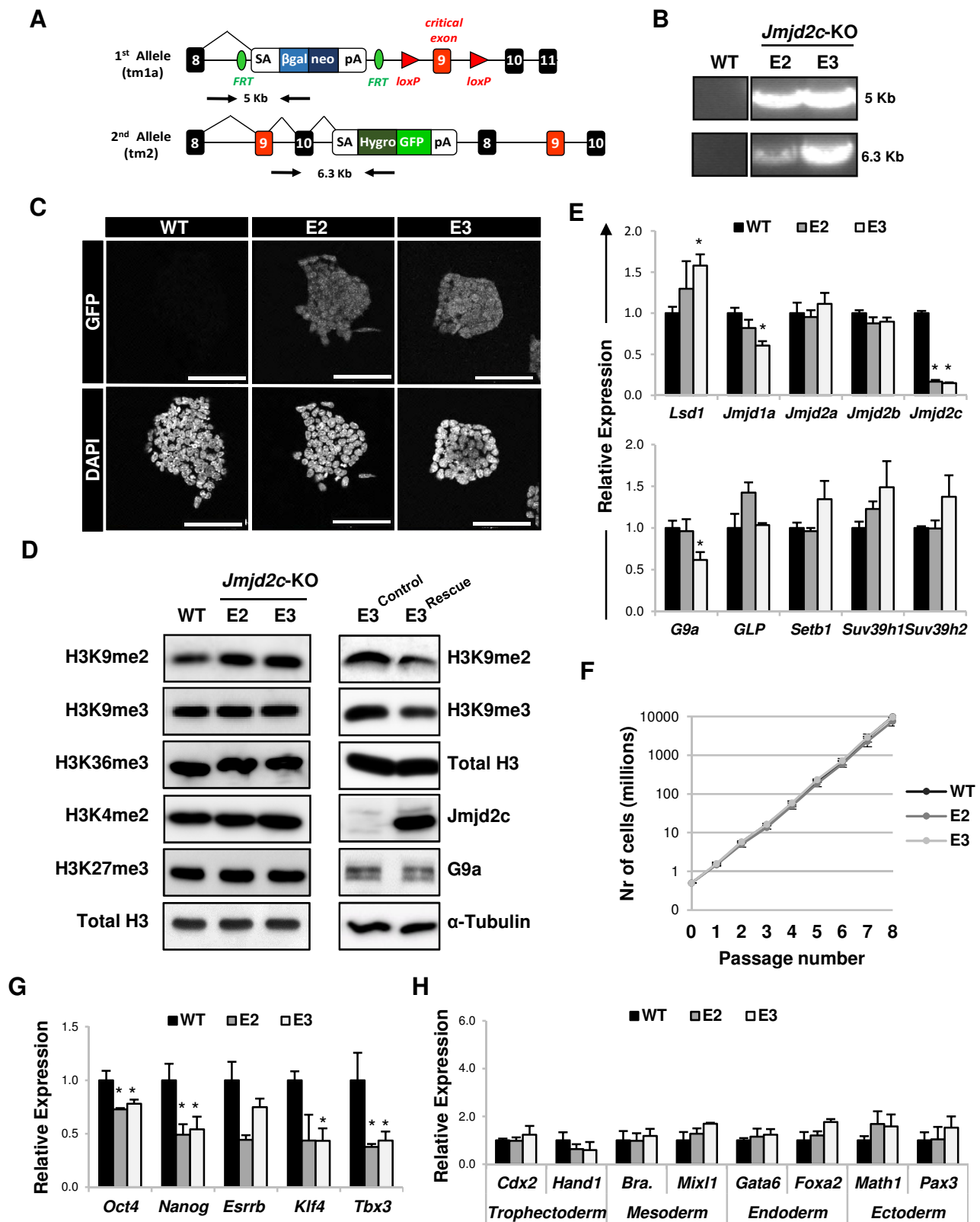


Fig.S1. Validation and characterization of *Jmjd2c*-knockout embryonic stem cell (ESC) clones. (A) Scheme showing *Jmjd2c* targeted alleles. Black boxes indicate exons and red boxes the critical exon 9, white boxes splice acceptor sequences (SA) or polyadenylation sequences (pA), blue (tm1a allele) and green (tm2 allele) boxes drug resistance (neomycin (neo), hygromycin (hyg)) and marker (lacZ and GFP) genes, green circles and red triangles show FRT and loxP sites, respectively. Opposing arrows indicate the position of primer pairs used for genotyping. (B) EtBr agarose gel showing long range PCR products of genomic DNA of wild-type (WT) and homozygous *Jmjd2c*-knockout (*Jmjd2c*-KO) JM8-ESC clones (E2, E3) using primers indicated in (A). Fragment sizes are indicated in kilobases. (C) Anti-GFP labelling and DAPI staining of WT and *Jmjd2c*-KO ESC clones. Bars, 100 μ m. (D) Western blot of acid-extracted histone lysates from WT and *Jmjd2c*-KO ESC clones (left panels) showing bulk levels of H3K9me2, H3K9me3, H3K36me3, H3K4me2, H3K27me3 and total H3. Western blot of acid-extracted histone lysates and whole cell extracts of *Jmjd2c*-KO ESC clone E3 transfected with an empty vector (Control) or with full-length *Jmjd2c* cDNA (Rescue) (right panels) showing bulk levels of H3K9me2, H3K9me3 and total H3 (upper lanes), and *Jmjd2c*, G9a and α -Tubulin (bottom lanes). (E) Relative expression levels of a panel of H3K9-demethylases (upper panel) and H3K9-methyltransferases (bottom panel) in WT and *Jmjd2c*-KO ESC clones grown in serum/LIF. (F) Growth curve of WT (ESC^{WT}) and *Jmjd2c*-KO (ESC^{*Jmjd2c*-KO}) clones E2 and E3 in self-renewing conditions over 8 passages (16 days). Plot represents an average of the cell number scored in 3 independent experiments. Error bars indicate \pm s.e.m. (G) Relative expression levels of the pluripotency-associated markers *Oct4*, *Nanog*, *Esrrb*, *Klf4* and *Tbx3* in WT and *Jmjd2c*-KO ESC clones. (H) Relative expression levels of differentiation markers associated to the trophectoderm (*Cdx2* and *Hand1*), mesoderm (*Brachyury* and *Mixl1*), endoderm (*Gata6* and *Foxa2*) and ectoderm (*Math1* and *Pax3*) lineages in WT and *Jmjd2c*-KO ESC clones. All expression data were normalised to two housekeeping genes, and expressed relative to WT as the mean \pm s.e.m. of at least three biological replicates. **P*<0.05; Mann-Whitney *U* test.

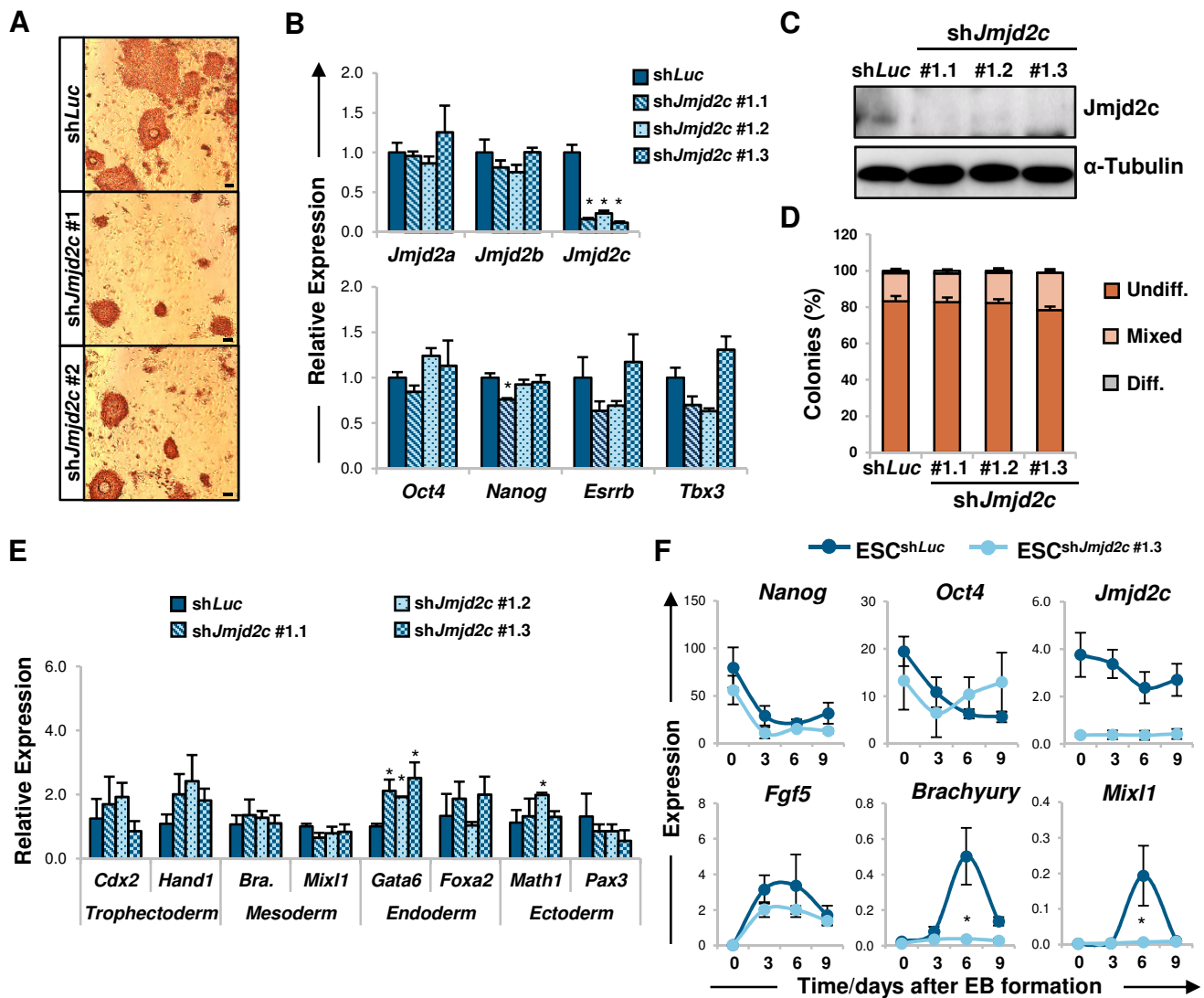


Fig. S2. Generation of embryoid bodies (EBs) is compromised in stable *Jmjd2c*-knockdown ESC clones. (A) E14-ESCs cells were transfected with two independent puromycin-selectable shRNA vectors targeting *Jmjd2c* (sh*Jmjd2c* #1 and #2) or a control vector (sh*Luc*) targeting *Luciferase* (Loh et al., 2007). Selection was maintained for 4 days, then cells were fixed and stained for alkaline phosphatase activity. Bars, 100 μ m. (B) Relative expression levels of *Jmjd2* family members and selected pluripotency-associated factors in three stable *Jmjd2c*-knockdown clones established from transfected ESCs with sh*Jmjd2c* #1 vector. Data were normalised to housekeeping genes, and expressed relative to a control ESC clone (sh*Luc*) as mean \pm s.e.m. of three biological replicates. * P <0.05; Mann-Whitney *U* test. (C) Western blot using anti-*Jmjd2c* antibodies on whole cell extracts of three stable *Jmjd2c*-knockdown ESC clones (sh*Jmjd2c* #1.1, #1.2 and #1.3) and a control clone (sh*Luc*). α -Tubulin is used as loading control. (D) Percentage of colonies scored as undifferentiated (Undiff.), mixed or differentiated (Diff.) according to the intensity of alkaline phosphatase staining of stable *Jmjd2c*-knockdown and control ESC clones. Each cell line was plated at low density and cultured for 5 days with LIF and serum. Data are the mean \pm s.e.m. of three biological replicates. (E) Relative expression levels of differentiation markers associated to the trophectoderm (*Cdx2* and *Hand1*), mesoderm (*Brachyury* and *Mixl1*), endoderm (*Gata6* and *Foxa2*) and ectoderm (*Math1* and *Pax3*) lineages in control (sh*Luc*) and *Jmjd2c*-knockdown (sh*Jmjd2c* #1.1, #1.2 and #1.3) ESC clones. Data were normalised to two housekeeping genes, and expressed relative to a control ESC clone (sh*Luc*) as mean \pm s.e.m. of three biological replicates. * P <0.05; Mann-Whitney *U* test. (F) Transcript levels of pluripotency-associated (*Nanog* and *Oct4*), *Jmjd2c*, and early differentiation markers for epiblast (*Fgf5*) and primitive streak (*Brachyury* and *Mixl1*) in sh*Jmjd2c* clone #1.3 and sh*Luc* control ESCs upon EB-induced differentiation. Similar results were obtained in sh*Jmjd2c* clone #1.2 and #1.1 ESCs (data not shown). Data were normalized to two housekeeping genes, and expressed as the mean \pm s.e.m. of at least three independent experiments. * P <0.05; Mann-Whitney *U* test.

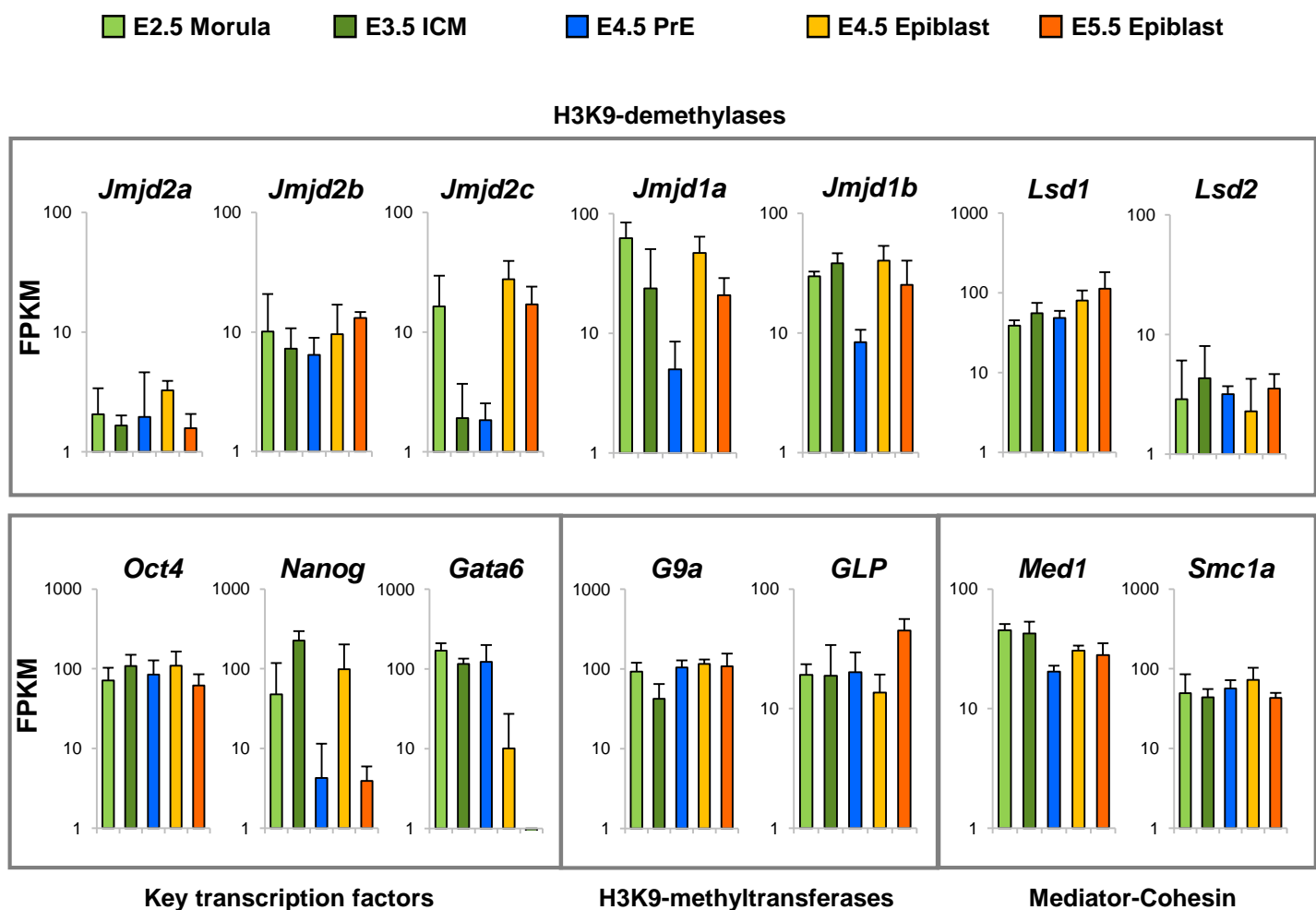


Fig. S3. *Jmjd2c* is dynamically expressed in the early mouse embryo. Comparative gene expression analysis at different developmental-times focussing on selected members of H3K9-demethylase families (*Jmjd2/Kdm4*: *Jmjd2a*, *Jmjd2b* and *Jmjd2c*; *Jmjd1/Kdm3*: *Jmjd1a* and *Jmjd1b*; *Kdm1*: *Lsd1* and *Lsd2*), epiblast (*Oct4* and *Nanog*) and primitive endoderm (*Gata6*) associated transcription factors, H3K9-methyltransferases (*G9a* and *GLP*) and the subunits of the Mediator (*Med1*) and Cohesin (*Smc1a*) complexes. Expression was assessed by RNA-seq in morula-stage embryos (E2.5), isolated inner cell mass (ICM) from early blastocysts (E3.5), dissected primitive endoderm (PrE) and epiblast layers from late blastocysts (E4.5) and in the post-implantation epiblast (E5.5), as previously published (Boroviak et al., 2015). Data are shown as the mean \pm s.d. of three independent pool samples in Fragments per Kilobase of Exon per Million Fragments (FPKM).

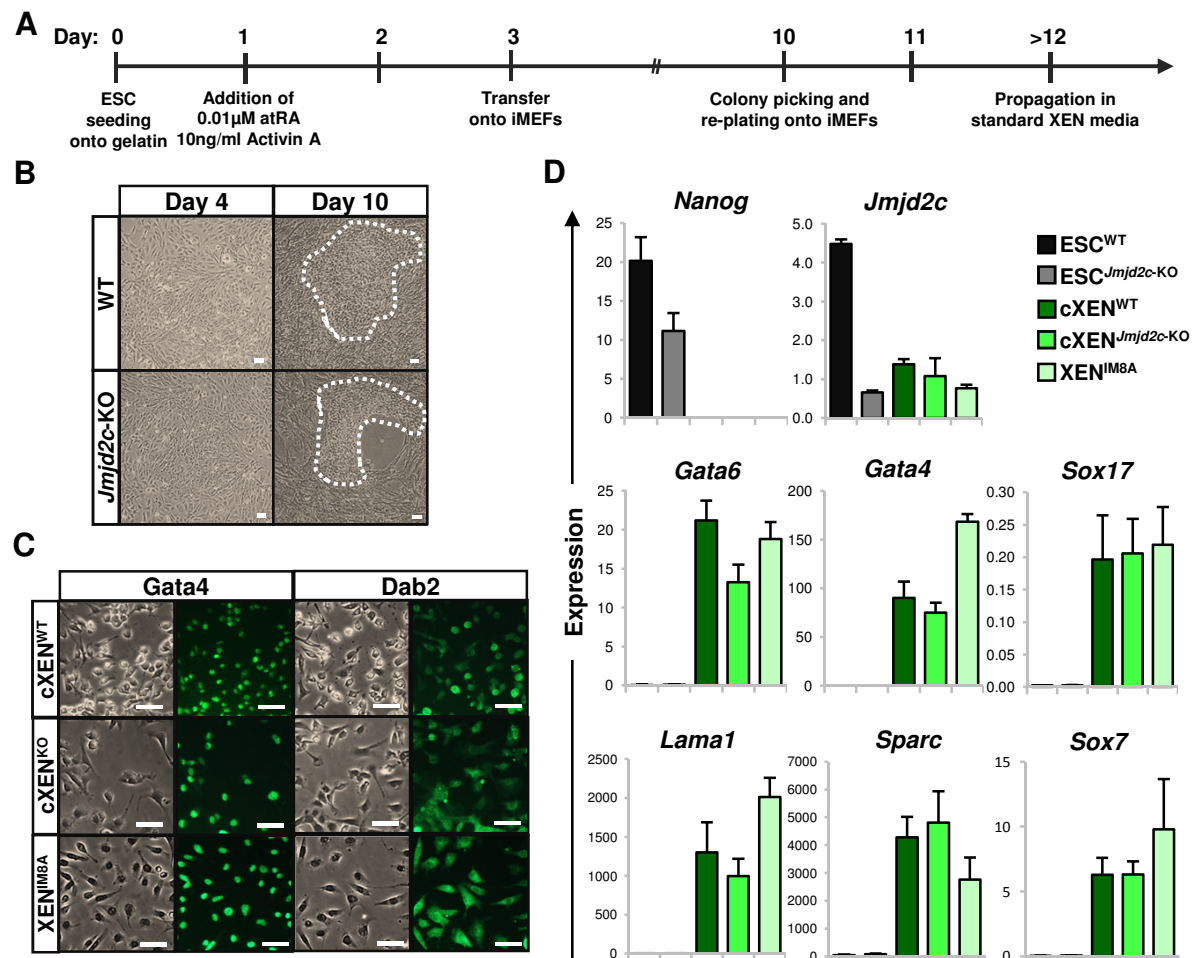


Fig. S4. *Jmjd2c*-knockout ESCs successfully generate self-renewing extra-embryonic endoderm (XEN) stem cells. (A-B) Timeline of ESC-to-XEN derivation protocol (adapted from Cho et al., 2012), and phase-contrast images of WT and *Jmjd2c*-KO ESC clone E3 cultures upon XEN cell conversion at the indicated time points. Bars, 100 µm. (C) Phase-contrast and staining for Gata4 and Dab2 of stably ESC-derived WT and *Jmjd2c*-KO converted XEN (cXEN) cells, and a control embryo-derived XEN cell line (IM8A). Bars, 100 µm. (D) Transcript levels of *Nanog*, *Jmjd2c* and XEN-associated markers (*Gata6*, *Gata4*, *Sox17*, *Lama1*, *Sparc* and *Sox7*) in WT and *Jmjd2c*-KO ESCs, cXEN cells, and embryo-derived XEN cells. Data were normalized to housekeeping genes, and expressed as the mean±s.e.m. of three biological replicates.

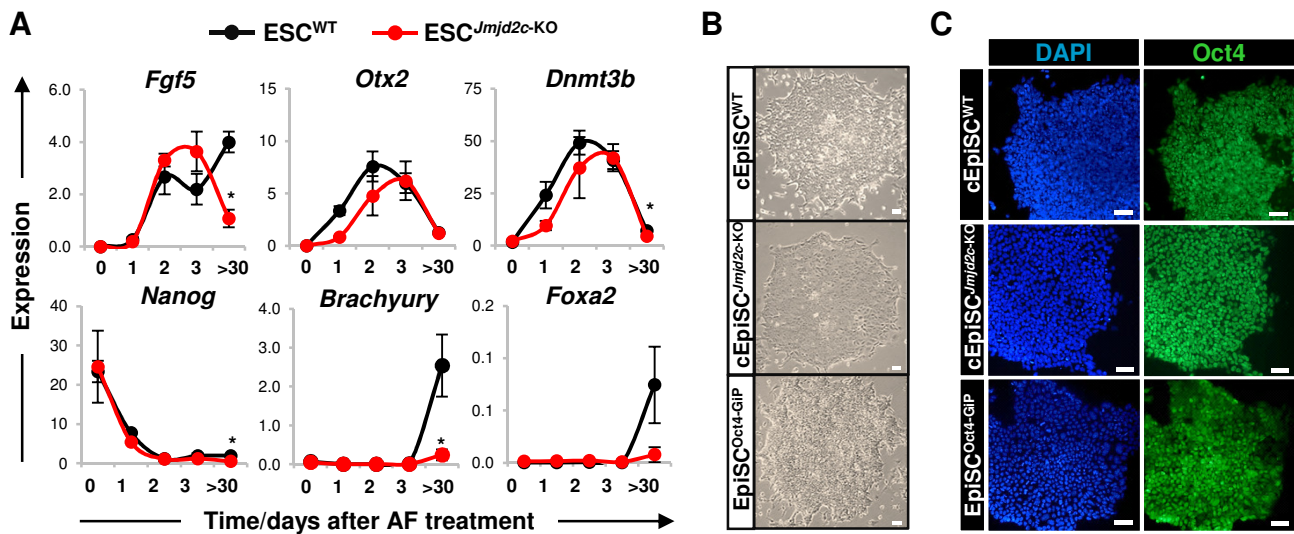


Fig. S5. *Jmjd2c*-knockout ESCs adopt an immature epiblast stem cell (EpiSC) phenotype. (A) Transcript levels of epiblast (*Fgf5*, *Otx2*, and *Dnmt3b*), pluripotency (*Nanog*) and differentiation (*Brachyury* and *Foxa2*) markers upon conversion of WT and *Jmjd2c*-KO ESCs into EpiSCs (day 0 to 3) and in stably converted EpiSCs (cEpiSCs; day >30) in the presence of Activin and Fibroblast growth factor (AF). Data were normalized to housekeeping genes, and expressed as the mean ± s.e.m. of at least three biological replicates. * $P < 0.05$; Mann-Whitney U test. (B) Phase-contrast images of stably derived cEpiSC cell lines from WT (cEpiSC^{WT}) and *Jmjd2c*-KO (cEpiSC^{*Jmjd2c*-KO}) clone E3 ESCs, and a control embryo-derived EpiSC line in which GFP expression is coupled with Oct4 (Oct4-GiP). Bars, 100 μ m. (C) Oct4 labelling and DAPI staining in stable WT and *Jmjd2c*-KO cEpiSCs, and in control embryo-derived EpiSCs^{Oct4-GiP}. Bars, 100 μ m.

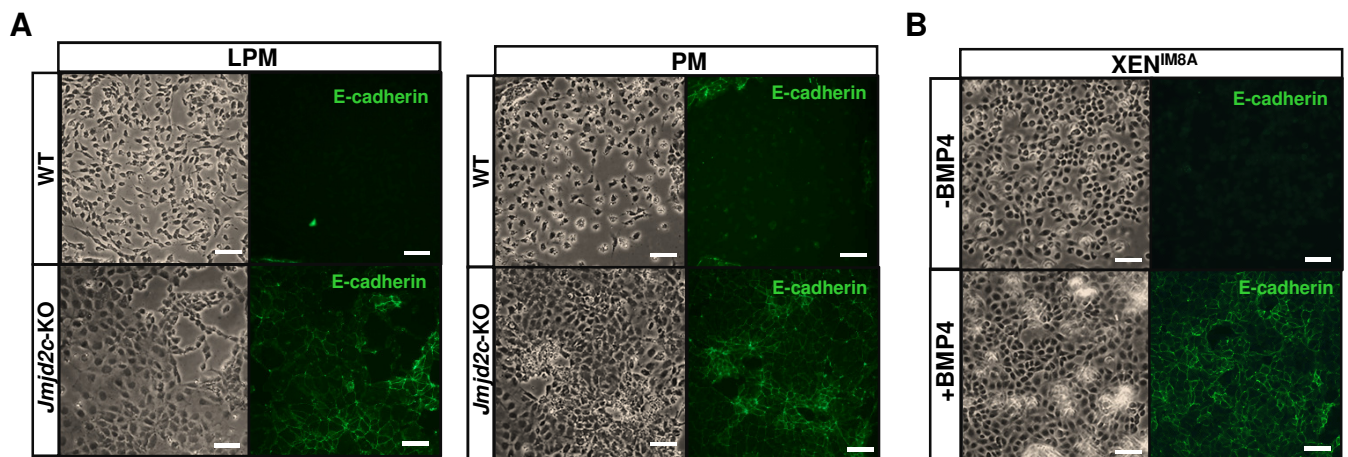


Fig. S6. Skewed differentiation into extra-embryonic endoderm (XEN)-like phenotype upon mesodermal induction of *Jmjd2c*-knockout cEpiSCs. Phase-contrast images and E-cadherin labelling of WT and *Jmjd2c*-KO cEpiSCs at day 4 of differentiation into lateral plate (LPM) and paraxial (PM) mesoderm cell types (A), and of XEN^{IM8A} cells with and without BMP4 treatment (B). Bars, 100 μm.

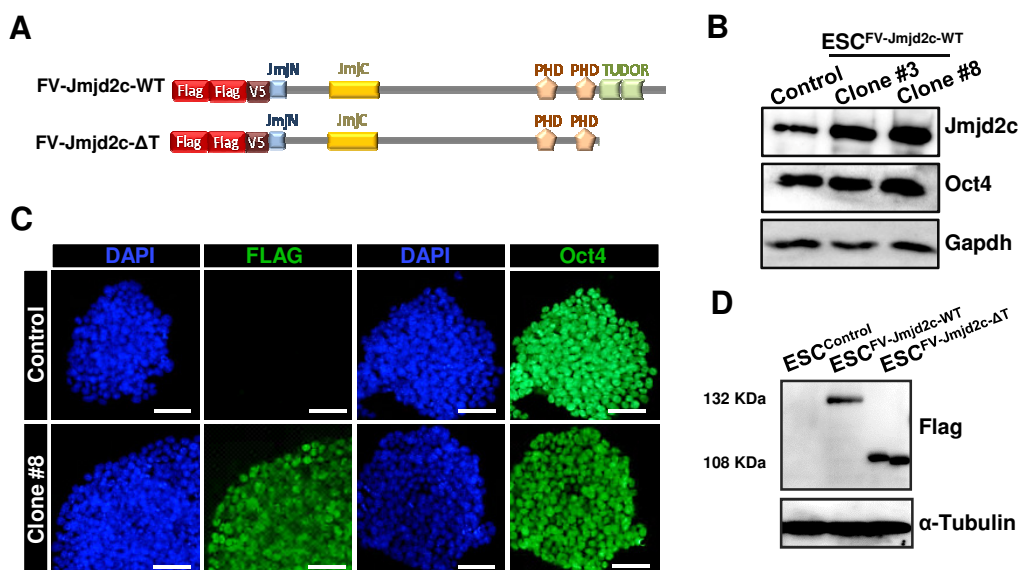


Fig. S7. Characterization of ESC clones stably expressing double-tagged wild-type and mutant Jmjd2c proteins. (A) Scheme of generated Flag(x2)-V5 tagged full-length wild-type (FV-Jmjd2c-WT) and mutated (FV-Jmjd2c-ΔT) Jmjd2c construct where both Tudor domains were deleted. Both constructs were used to generate stable ESC lines. An empty version of the same construct (without Jmjd2c) was used to generate a control ESC line. (B) Western blot of whole cell extracts of independent FV-Jmjd2c-WT (clone#3 and #8) and control ESC clones showing Jmjd2c and Oct4 protein levels. Gapdh was used as a loading control. (C) Labelling of the Flag epitope or Oct4 (green), and DAPI staining (blue) in control and FV-Jmjd2c-WT clone#8 ESCs. Bars, 100 μm. (D) Western blot showing protein levels of the Flag epitope in FV-Jmjd2c-WT clone#3 (132 KDa) and FV-Jmjd2c-ΔT clone#1 (108 KDa) ESC lines. α-Tubulin was used as a loading control.

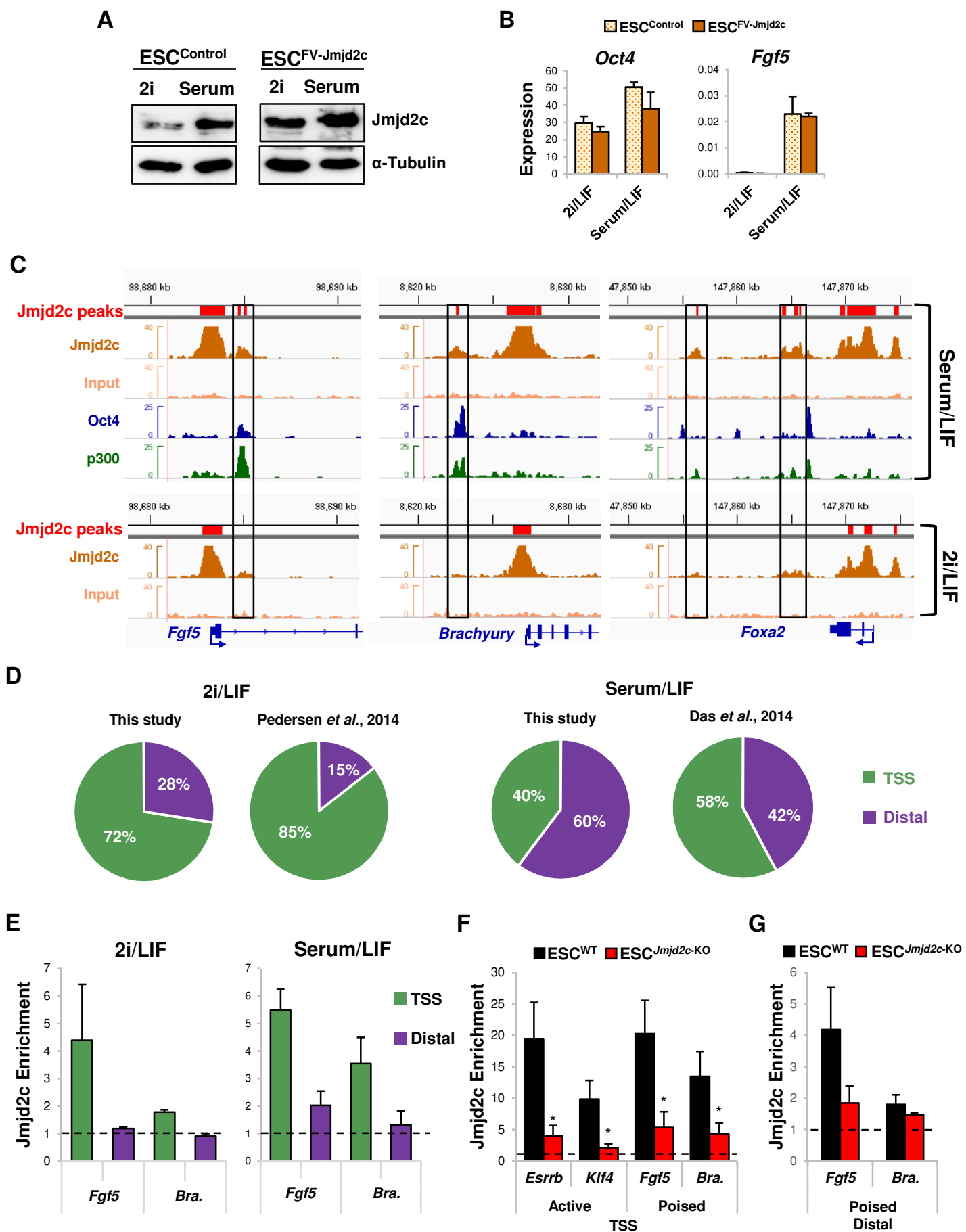


Fig. S8. Jmjd2c is re-distributed to lineage-specific enhancers during the priming of ESCs for differentiation. (A) Western blot showing Jmjd2c protein levels in control and FV-Jmjd2c-WT clone #8 ESCs cultured in either 2i/LIF or serum/LIF conditions. α -Tubulin was used as a loading control. (B) Expression of the pluripotency (*Oct4*) and early epiblast-associated (*Fgf5*) genes in control and FV-Jmjd2c-WT ESCs routinely cultured in 2i/LIF and serum/LIF showing the detection of *Fgf5* transcript in primed (serum/LIF) ESC cultures in contrast to naïve (2i/LIF) cells. Data were normalized to housekeeping genes, and expressed as the mean \pm s.e.m. of three biological replicates. (C) ChIP-seq binding profiles showing Jmjd2c peaks at the TSS regions of the lineage-specific *Fgf5*, *Brachyury* and *Foxa2* genes in 2i/LIF conditions (bottom panel), and the acquisition of additional Jmjd2c peaks overlapping with p300 and Oct4 at distal sites in the vicinity of the same genes in serum/LIF conditions (top panel). (D) Percentage of Jmjd2c-bound TSS (green) and distal (purple) peaks detected in primed (serum/LIF) and naïve (2i/LIF) conditions using datasets generated in this study and in previously published reports as indicated. (E) Enrichment levels for endogenous Jmjd2c binding at TSS and distal (enhancer) regions of *Fgf5* and *Brachyury* loci in formaldehyde-fixed chromatin from wild-type JM8-ESCs routinely cultured in 2i/LIF and serum/LIF conditions. Data were expressed as average fold enrichment over negative control region (intergenic; dotted line), and represent the mean \pm s.e.m. of three independent experiments. (F) Specificity of endogenous Jmjd2c ChIP was validated by assessing enrichment for Jmjd2c at active (*Esrrb* and *Klf4*) and poised (*Fgf5* and *Brachyury*) TSS regions extracted from wild-type (WT) JM8-ESCs and *Jmjd2c*-knockout (*Jmjd2c*-KO) ESCs. Data were expressed as average fold enrichment over negative control region (intergenic; dotted line), and represent the mean \pm s.e.m. of three independent experiments. (G) Enrichment levels of endogenous Jmjd2c binding at distal regions of *Fgf5* and *Brachyury* in WT versus *Jmjd2c*-KO ESCs. Data were expressed as average fold enrichment over negative control region (intergenic; dotted line), and represent the mean \pm s.e.m. of three independent experiments. * P <0.05; Mann-Whitney U test.

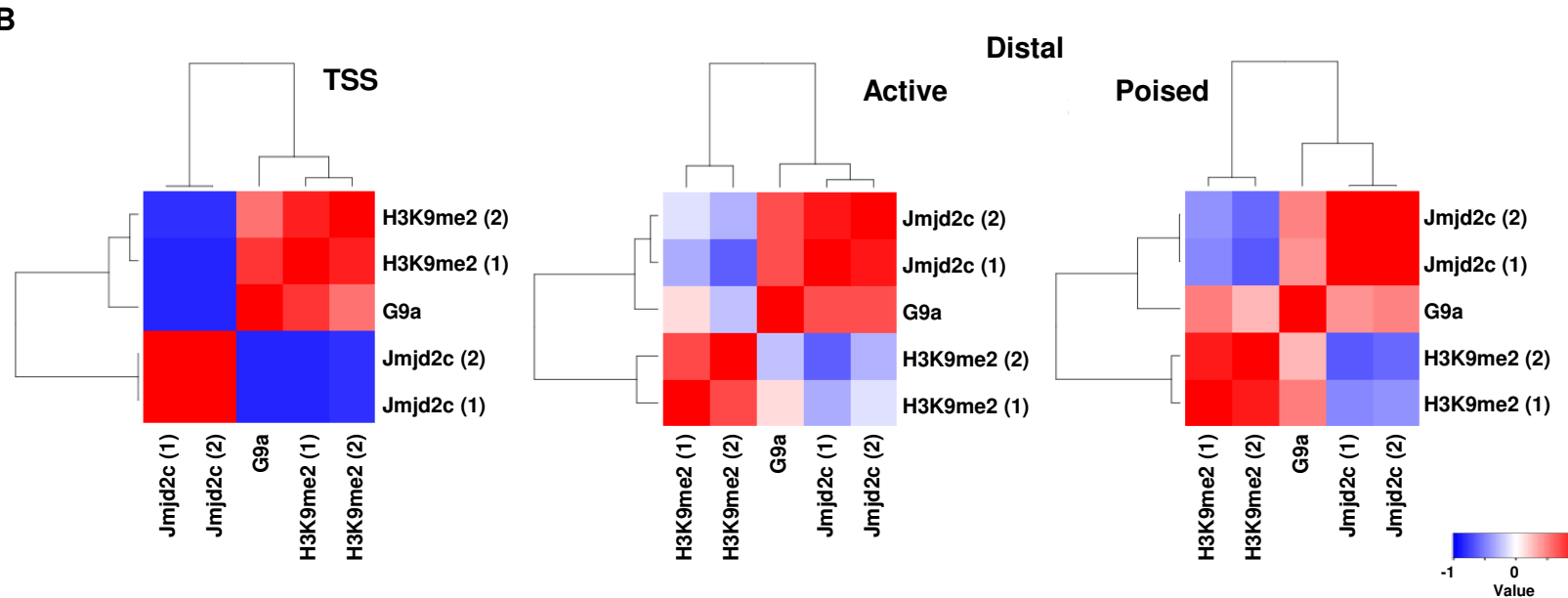
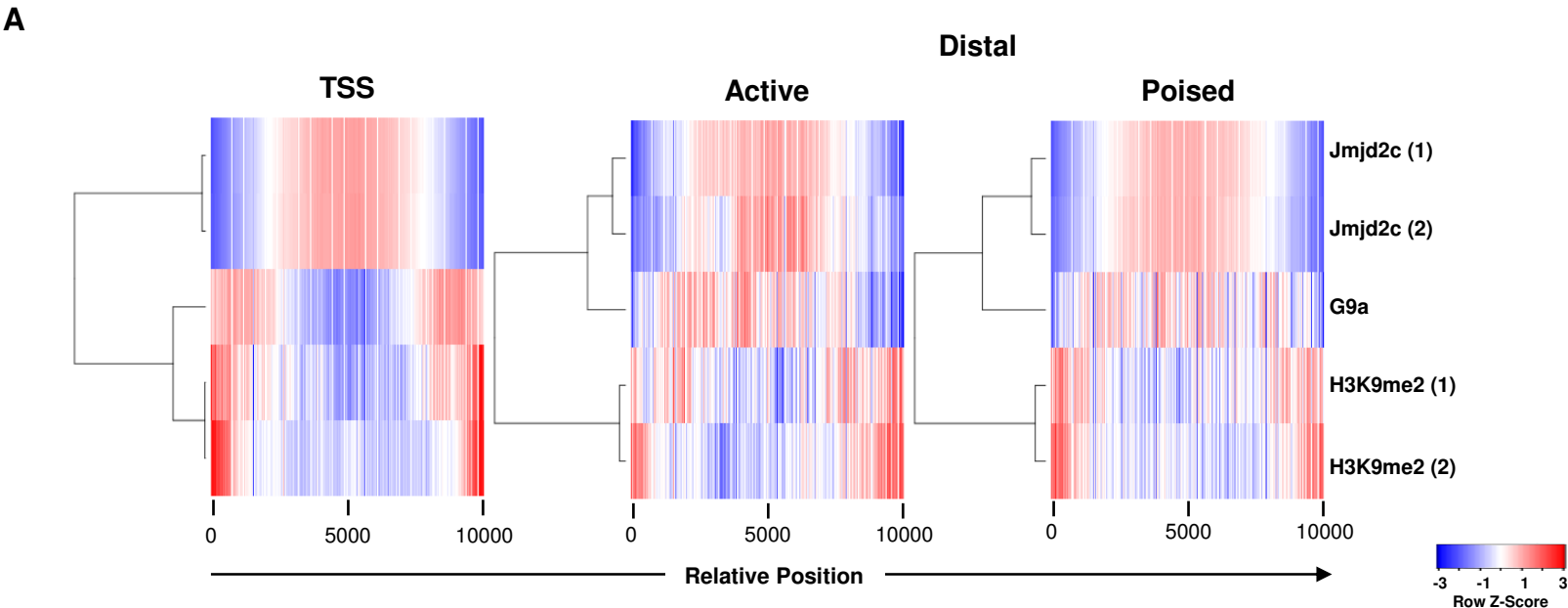


Fig. S9. G9a and Jmjd2c overlap genome-wide in ESCs at both active and poised enhancer regions in the absence of H3K9me2 deposition. (A) Heatmap representation of the distribution (i.e. binned mean ChIP-seq read density) of Jmjd2c (1: this study; 2: Das et al., 2014), G9a (Mozzetta et al., 2014), H3K9me2 (1: Liu et al., 2015; 2: Das et al., 2014) across Jmjd2c-bound TSS or active and poised distal sites. Each ChIP-seq experiment was adjusted for sequencing depth and normalised to their respective input. The colour key from blue to red indicates the enrichment levels from low to high, respectively. (B) Heatmap showing Pearson correlation between the distributions of Jmjd2c (1: this study; 2: Das et al., 2014), G9a (Mozzetta et al., 2014), H3K9me2 (1: Liu et al., 2015; 2: Das et al., 2014) across Jmjd2c-bound TSS or active and poised distal sites. The colour key from blue to red indicates the correlation coefficient from low to high, respectively.

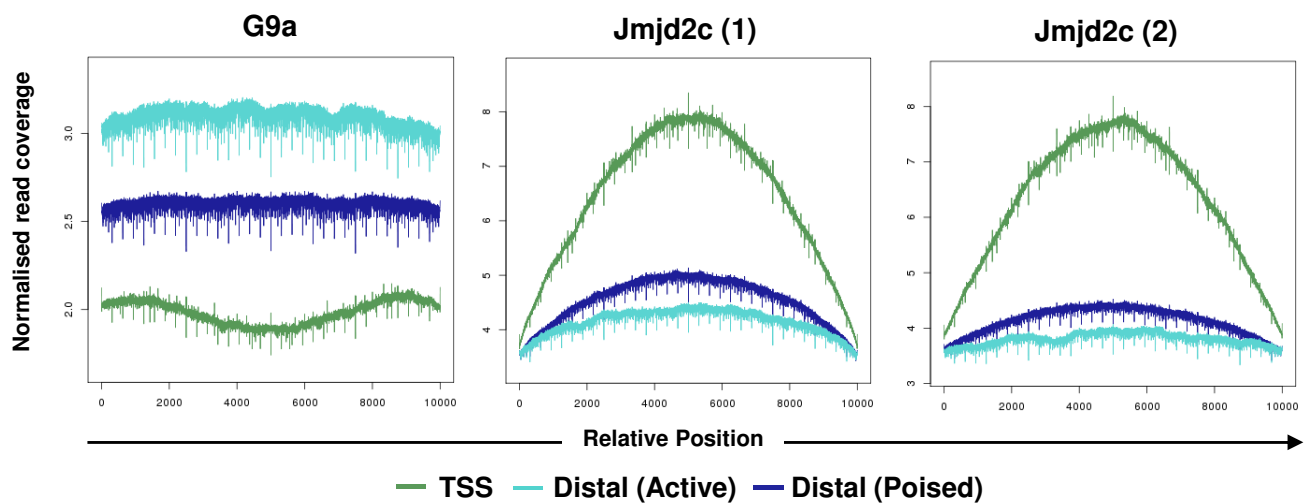
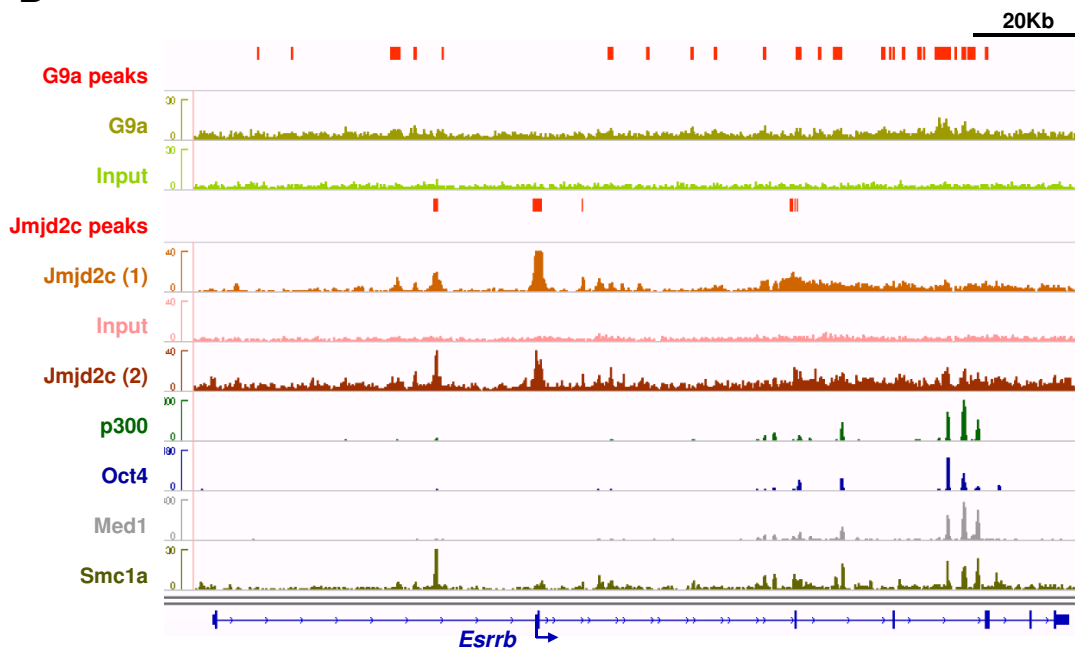
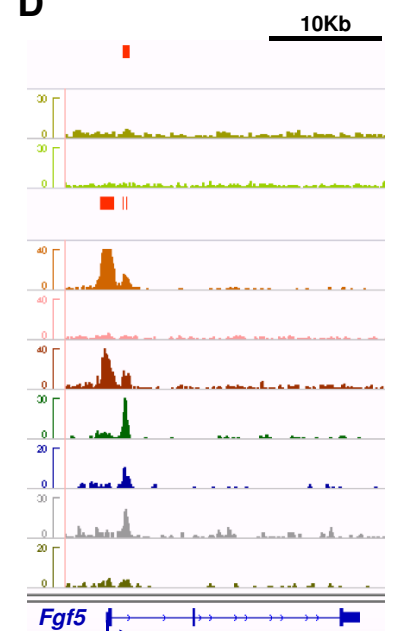
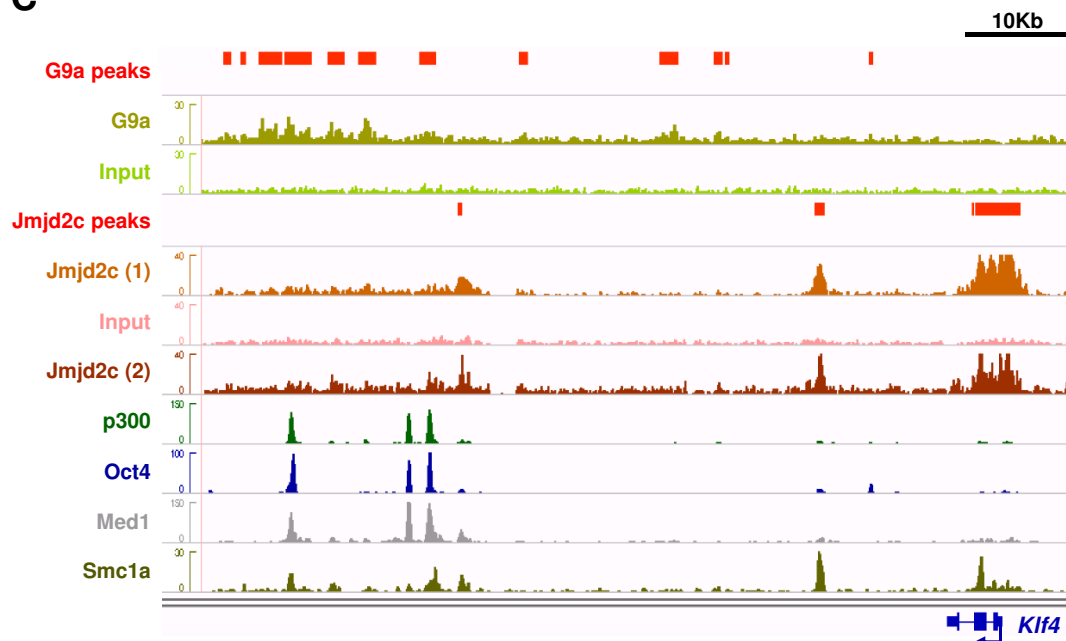
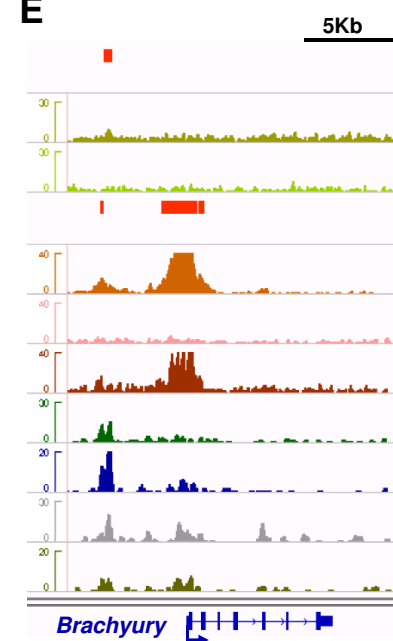
A**B****D****C****E**

Fig. S10. G9a highest density binding is observed at Jmjd2c-bound active enhancer regions in ESCs. (A) Coverage plot representation of the distribution (i.e. binned mean ChIP-seq read density) of G9a (Mozzetta et al., 2014) and Jmjd2c (1: this study; 2: Das et al., 2014) at Jmjd2c-bound TSS (green), distal active (light blue) and distal poised (dark blue) sites. Each ChIP-seq experiment was adjusted for sequencing depth and normalised to their respective input. (B) ChIP-seq binding profiles for G9a (Mozzetta et al., 2014) and Jmjd2c (1: this study; 2: Das et al., 2014), alongside with published profiles for the enhancer-associated factors p300, Oct4, Med1 and Smc1a, at the active enhancer regions of *Esrrb* (B) and *Klf4* (C) loci, and the poised enhancers of *Fgf5* (D) and *Brachyury* (D) loci. Red bars represent peaks called relative to respective input control samples for G9a (Mozzetta et al., 2014) and Jmjd2c (this study) ChIP-seq datasets.

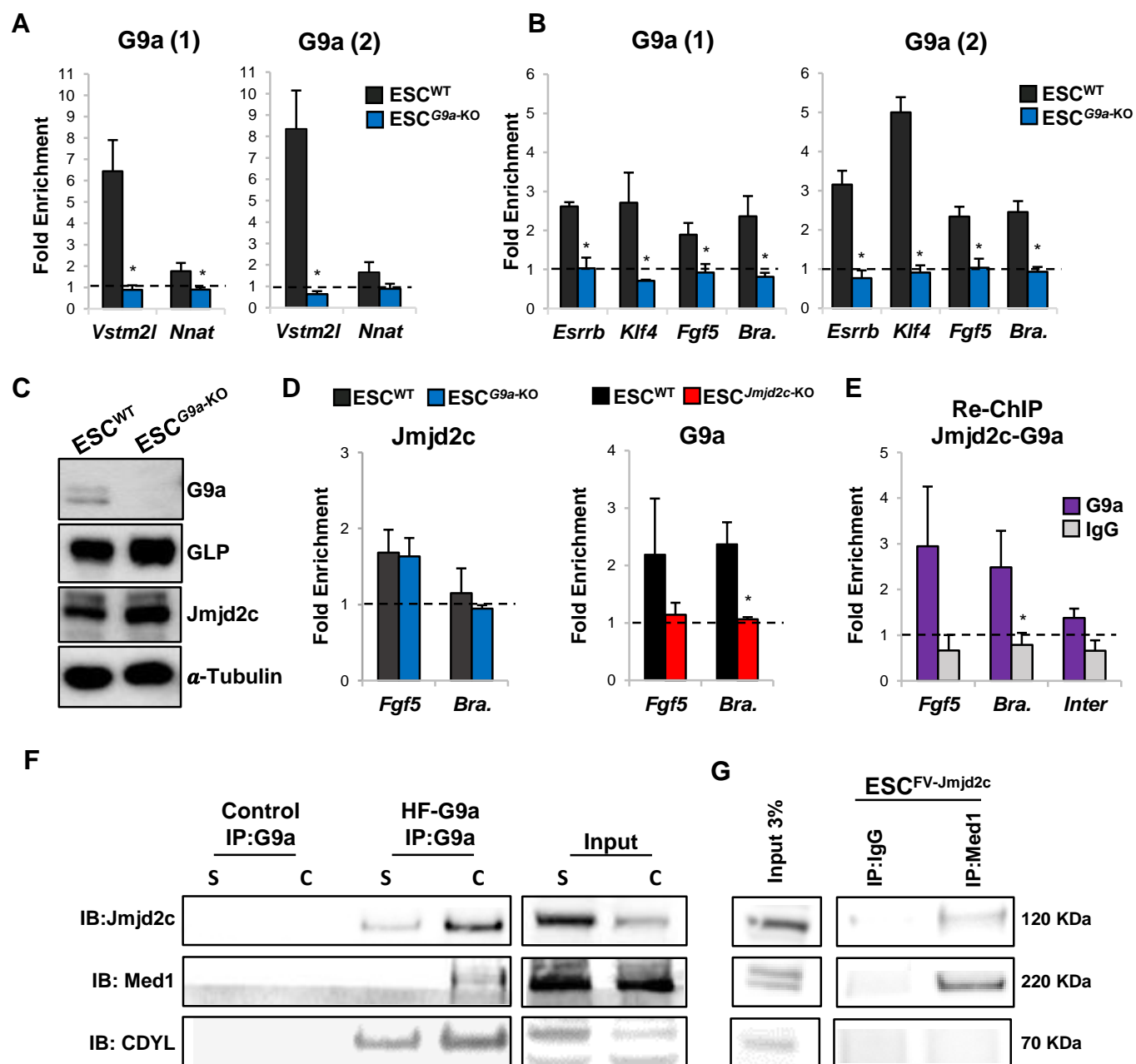


Fig. S11. Jmjd2c facilitates G9a binding at lineage-specific enhancers in ESCs.

(A) Specificity of two anti-G9a antibodies (1: Cell Signalling; 2: R&D) was validated in ChIP-qPCR by assessing enrichment levels for G9a at previously reported regions with high (*Vstm2l*) and low (*Nnat*) enrichment in wild-type (WT) TT2-ESCs and *G9a*-knockout (*G9a*-KO) in serum/LIF conditions. Data were expressed as average fold enrichment over negative control region (intergenic; dotted line), and represent the mean \pm s.e.m. of three independent experiments. * P <0.05; Mann-Whitney U test. (B) Specificity of anti-G9a antibodies (1: Cell Signalling; 2: R&D) was also validated in ChIP-qPCR by assessing enrichment levels for G9a at the enhancer regions of active (*Esrrb* and *Klf4*) and transcriptionally primed (*Fgf5* and *Brachyury*) genes in WT and *G9a*-KO ESCs in serum/LIF conditions. Data were expressed as average fold enrichment over negative control region (intergenic; dotted line), and represent the mean \pm s.e.m. of three independent experiments. * P <0.05; Mann-Whitney U test. (C) Western blot using anti-G9a, anti-GLP and anti-Jmjd2c antibodies of whole cell extracts from WT and *G9a*-KO ESCs. α -Tubulin was used as a loading control. (D) Enrichment levels for endogenous Jmjd2c at *Fgf5* and *Brachyury* enhancer regions in WT and *G9a*-KO ESCs (left panel). Enrichment levels for G9a at *Fgf5* and *Brachyury* enhancer regions in wild-type (WT) JM8-ESCs and *Jmjd2c*-knockout (*Jmjd2c*-KO) (right panel). Data were expressed as average fold enrichment over negative control region (intergenic; dotted line), and represent the mean \pm s.e.m. of three independent experiments. (E) Co-binding of Jmjd2c and G9a was validated at *Fgf5* and *Brachyury* enhancer regions by sequential ChIP (Re-ChIP) in ESCs expressing Flag-tagged Jmjd2c. Jmjd2c was immunoprecipitated using anti-Flag antibodies, followed by immunoprecipitation with anti-G9a (R&D), IgG or beads only. An intergenic region was included to confirm background levels. Data were expressed as fold enrichment over beads only control (dotted line), and represent the mean \pm s.e.m. of three independent experiments. * P <0.05; Mann-Whitney U test. (F) G9a interaction partners were purified with a double immunoprecipitation (IP) with anti-Flag and anti-HA antibodies in soluble (S) and chromatin (C) nuclear fractions of HeLa cells expressing an empty vector (Control) or tagged (HF-G9a) G9a protein. (G) Med1 immunoprecipitation was performed in nuclear fractions of ESCs expressing a Flag-tagged Jmjd2c (FV-Jmjd2c). Interactions were visualised by immunoblotting (IB) with anti-Med1, anti-Jmjd2c or anti-CDYL antibodies. Data are representative of duplicate experiments. The input and IgG lanes of Jmjd2c correspond to the same experiment as Figure 5D.

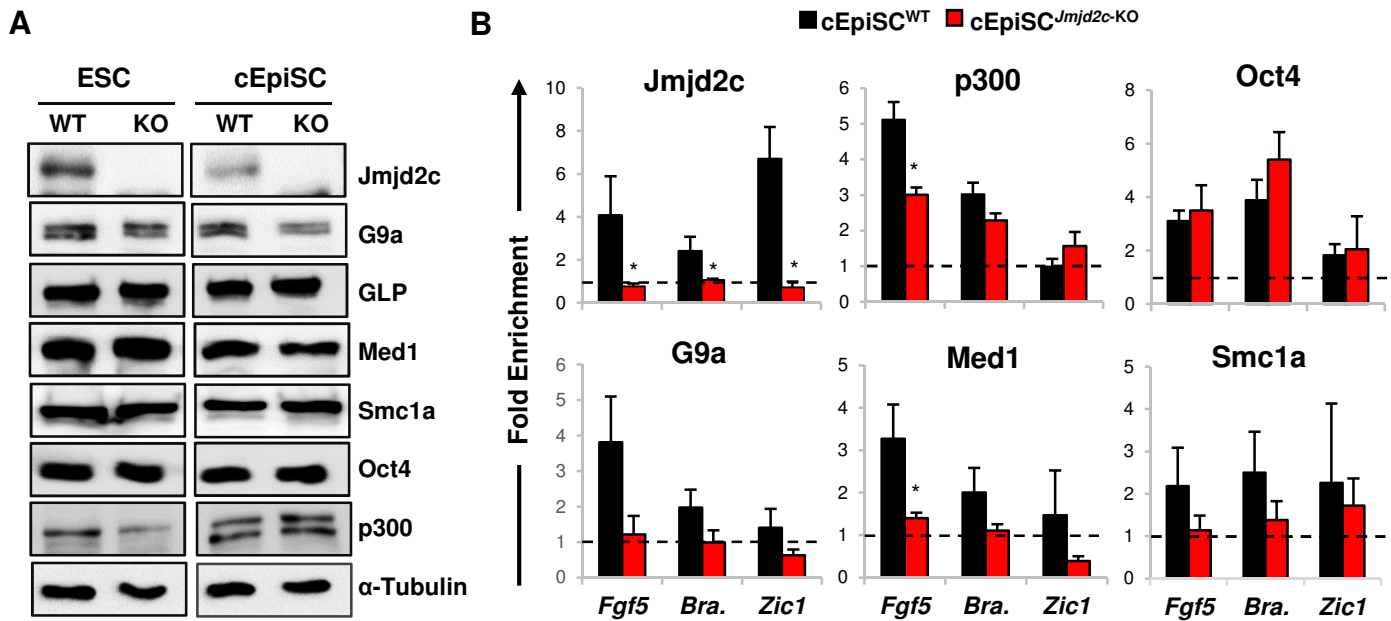


Fig. S12. Loss of Jmjd2c compromises G9a, Med1 and Smc1a binding at Oct4-bound poised enhancers in ESC-derived cEpiSCs. (A) Western blot using antibodies against Jmjd2c, G9a, GLP, Med1, Smc1a, Oct4 and p300 in whole cell extracts from wild-type (WT) JM8-ESCs, *Jmjd2c*-knockout (*Jmjd2c*-KO) ESCs and derived cEpiSCs. α -Tubulin was used as a loading control. (B) Enrichment levels for Jmjd2c, p300, Oct4, G9a, Med1 and Smc1a at the active *Fgf5* (PE) and poised *Brachyury* and *Zic1* enhancers as assessed by ChIP-qPCR in WT and *Jmjd2c*-KO cEpiSCs. Data were expressed as average fold enrichment over negative control region (intergenic; dotted line), and represent the mean \pm s.e.m. of three independent experiments. * $P < 0.05$; Mann-Whitney U test.

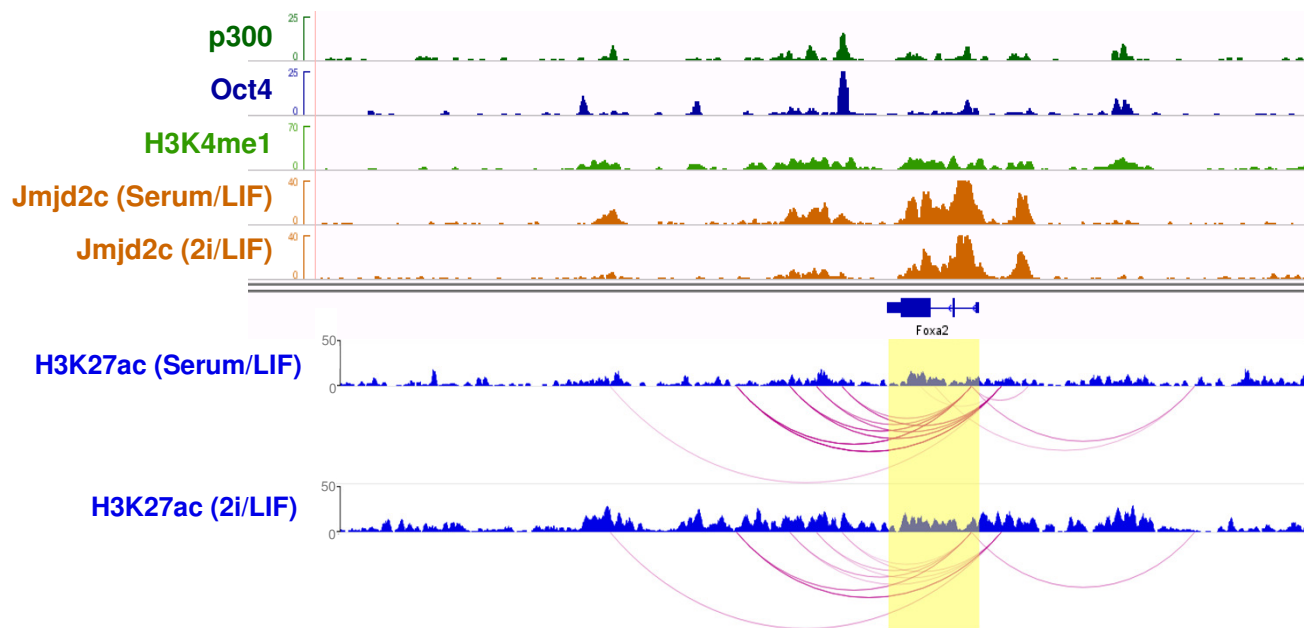


Fig. S13. Chromatin dynamics across *Foxa2* locus in naïve (2i/LIF) and primed (serum/LIF) ESCs. ChIP-seq binding profiles showing p300, Oct4, H3K4me1 and Jmjd2c in either serum/LIF or 2i/LIF conditions across the *Foxa2* locus (top panel). Interaction profile for the promoter of *Foxa2* visualized for ESCs grown in either serum/LIF or 2i/LIF conditions (bottom panel). Pink arcs represent interactions from *Foxa2* promoter identified using CHiCAGO pipeline (Cairns et al., 2015) based on newly generated high coverage capture Hi-C datasets (O. Joshi, H.G. Stunnenberg, unpublished). The depth of pink colour of each interaction arc represents the strength of the interaction.

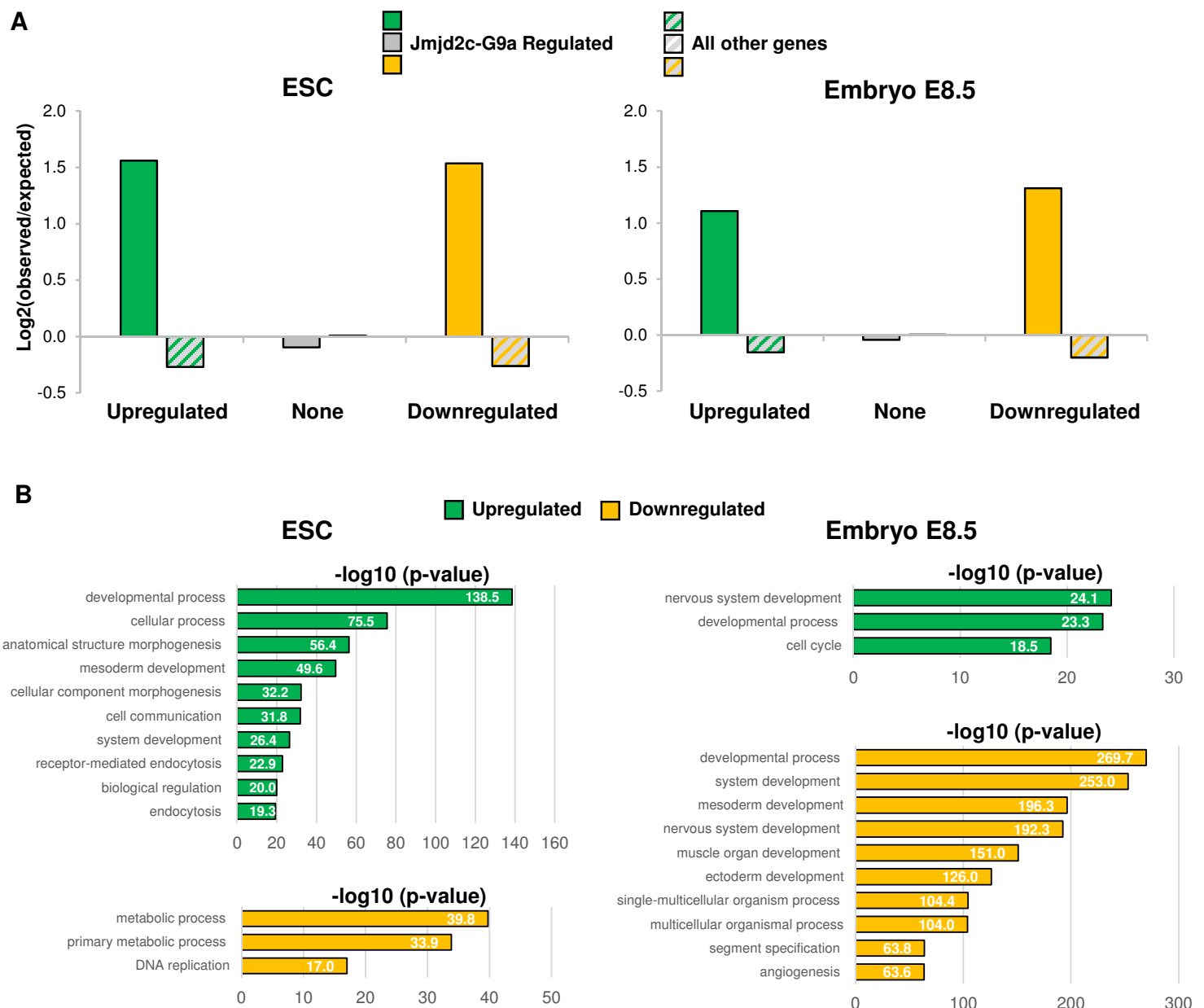


Fig. S14. Jmjd2c-G9a co-bound developmental genes are downregulated in the embryo in the absence of *G9a*. (A) Enrichment of Jmjd2c-G9a regulated genes amongst genes differentially expressed in *G9a*-knockout ESCs and embryos at E8.5.

Upregulated (\log_2 fold-change >0 , q -value <0.05) and downregulated (\log_2 fold-change <0 , q -value <0.05) genes were defined from publicly available RNA-seq datasets profiling gene expression in ESCs (GSE) and E8.5 embryos (GSE) with and without *G9a* knockout (Auclair et al., 2016; Mozzetta et al., 2014). Expected numbers in each set were calculated from the proportions of all measured genes belonging to each category (upregulated, downregulated, and none). Difference of observed numbers from expected were evaluated with Chi-squared test giving P -value = $3.10\text{E-}93$ and $1.00\text{E-}83$ in ESC and E8.5 embryo samples, respectively. (B) Top 10 most significant biological processes of Jmjd2c-G9a regulated genes that are either up (green) or downregulated (yellow) in *G9a*-knockout ESCs (left panel) or *G9a*-knockout embryos at E8.5 (right panel).

Table S1. Antibodies used in this study

Primary Antibody	Catalogue Number	Supplier	Concentration/Quantity		
			Western Blot	IF	ChIP
Cdyl	ab5188	Abcam	1:1000	-	-
Dab2	sc13982	SantaCruz	-	1:250	-
E-Cadherin	U3254	Sigma-Aldrich	-	1:500	-
Flag M2	F1804	Sigma-aldrich	1:1000	1:500	10 µg
G9a	3306	Cell Signalling	1:1000	-	0.24 µg
G9a	PP-A8620A-00	R&D	-	-	5 µg
Gata4	sc-9053	SantaCruz	-	1:250	-
Gata6	AF1700	R&D Systems	-	1:500	-
GFP	ab290	Abcam	-	1:1000	-
GLP	PP-B0422-00	R&D Systems	1:1000	-	-
H3	ab1791	Abcam	1:50,000	-	-
H3K27ac	ab4729	Abcam	-	-	5 µg
H3K27me3	07-449	Millipore	1:100,000	-	-
H3K36me3	mAb-183-050	Diagenode	1:10,000	-	-
H3K4me2	07-030	Millipore	1:50,000	-	-
H3K9me2	ab1220	Abcam	1:20,000	-	2 µg
H3K9me3	ab8898	Abcam	1:100,000	-	-
Jmjd2b	A301-478A	Bethyl Laboratories	1:2000	-	-
Jmjd2c	-	H.H. Ng's lab	1:2000	-	-
Jmjd2c	sc-104949	SantaCruz	1:1000	-	5 µg
Med1	A300-793A	Bethyl Laboratories	1:1000	-	8 µg
Oct4	sc-8628	SantaCruz	1:1000	-	5 µg
Oct4	sc-5279	SantaCruz	-	1:200	-
p300	sc-585	SantaCruz	1:1000	-	5 µg
Phalloidin	P1951	Sigma-Aldrich	-	1:100	-
Smc1a	A300-055A	Bethyl Laboratories	1:1000	-	8 µg
α-Tubulin	T6074	Sigma-Aldrich	1:20,000	-	-

Table S2. Sequences of primers used for genotyping

Name	Sequence (5' – 3')	Allele
tm1a-F	GAAGTAGGAGGAGAACCATAGTTCCAGAG	First
tm1a-R	GCCTCTTCGCTATTACGCCAGCTG	
tm2-F	AAGAGGTAAGAAGCCCATCACATC	Second
tm2-R	GCAGCTATTTACCCGCAGGA	

Table S3. Sequences of primers used for cloning of Jmjd2c

Name	Sequence (5' – 3')	Vector
XhoI-Jmjd2c-F	ATACATTCTCGAGATGGAGGTGGT	pPy-CAG-Jmjd2c
PacI-Jmjd2c3-R	CTCTTAATTAACACTGTCTCTTCTGACACT	
BamHI-Jmjd2c-F	ATTAGGATCCGAGGTGGTGGAGGTG	FV-Jmjd2c-WT
Sall-Jmjd2c-R	TAATGTCGACCTACTGTCTCTTCTGACACTT	
Sall-Del-Tudor-R	TAATGTCGACCTACGCGTTTGAGTTGAC	FV-Jmjd2c-ΔT

Table S4. Sequences of primers used for RT-qPCR

Gene	Forward (5' – 3')	Reverse (5' – 3')
<i>Oct4</i>	CGTGGAGACTTTGCAGCCTG	GCTTGGAAACTGTTCTAGCTCCT
<i>Brachyury</i>	CCGGTGCTGAAGGTAAATGT	CCTCCATTGAGCTTGTGGT
<i>Brachyury*</i>	TCAGCAAAGTCAAACCTCACC	TCATTCTGGTAGGCAGTCAC
<i>Cxcr4</i>	CGGGATGAAAACGTCCATTT	ATGACCAGGATCACCAATCCA
<i>Dnmt3b</i>	TTCAGTGACCAGTCCTCAGACACGAA	TCAGAAGGCTGGAGACCTCCCTCTT
<i>Setb1</i>	GAGGCCGGGAGAGGCTGAA	TAGCTGGTCGGCGAAGCCCT
<i>Esrrb</i>	GCACCTGGGCTCTAGTTGC	TACAGTCCTCGTAGCTCTTGC
<i>Fgf5</i>	TGTGTCTCAGGGGATTGTAGG	AGCTGTTTTCTTGAATCTCTC
<i>Fgf5*</i>	ACGTTTTCTTCTGTTCTTCTGC	TTCTTACAATCCCCTGAGAC
<i>Flk-1</i>	GACGGAGAAGGAGTCTGTGC	TTTCTGTGTGCTGAGCTTGG
<i>Foxa2</i>	CCATCAGCCCCACAAAATG	CCAAGCTGCCTGGCATG
<i>Foxa2*</i>	ACTGGAGCAGCTACTACGC	AGGATGACATGTTTATGGAG
<i>G9a</i>	TCACCCTGACTGACAATGAG	AGACAGGAACAACAGAACAC
<i>Gapdh</i>	AGAAGGTGGTGAAGCAGGCA	CGAAGGTGGAAGAGTGGGAG
<i>Gata4</i>	GAACACCCTGAGCAGGCCTC	TTTCTGGGAAACTGGAGCTGG
<i>Gata6</i>	GAGCTGGTGCTACCAAGAGG	TGCAAAAGCCCATCTCTTCT
<i>GLP</i>	CAGATGGAGAAACAAATGGGTCT	TTTGCTTCCCCACTTCTGTGT
<i>Hmbs</i>	ACTGGTGGAGTATGGAGTCTAGATGGC	GCCAGGCTGATGCCAGGTT
<i>Isl1</i>	AGACCCTCTCAGTCCCTTG	CGTCATCTCCACTAGTTGCTC
<i>Jmjd1a</i>	GAGCCACAGTCGGAGACTTC	TTGGCCATCAGATCATCAAA
<i>Jmjd2a</i>	TTCTGTGAATCCTGCGTCTG	TAGCTGTGCACGGTGAGAAC
<i>Jmjd2b</i>	CATGTGGAAGACCACGTTTG	AAGGGGATGCCGTACTTCTT
<i>Jmjd2c</i>	GATGACTGGCCTTACGTGGT	CTTCACACAGTTTCGGCTCA
<i>Klf4</i>	GTGCCCCGACTAACCCTTG	GTCGTTGAACTCCTCGGTCT
<i>L19</i>	TGATCTGCTGACGGAGTTG	GGAAAAGAAGGTCTGGTTGGA
<i>Lrp2</i>	CCTTGCCAAACCCTCTGAAAAT	CACAAGGTTTGCAGTGTCTTTA
<i>Lsd1</i>	GATGATGTCTGGGAAACAGG	GGGCCAAGGTAGAATACAGAG
<i>Math1</i>	GGAGAAGCTTCGTTGCACGC	GGGACATCGCACTGCAATGG
<i>Meox1</i>	ACGGAGAAGAAATCATCCAG	GTAGTTGTGGTGGGCAAAC
<i>Mixl1</i>	GACAGACCATGTACCCAGAC	GCTTCAAACACCTAGCTTCAG
<i>Nanog</i>	CTTACAAGGGTCTGCTACTGA	TCTGCTTCCCTGGCAAGGACC
<i>Otx2</i>	TATCTAAAGCAACCGCCTTACG	AAGTCCATAACCGAAGTGGTC
<i>Pax3</i>	GGGAACTGGAGGCATGTTTA	GTTTTCCGTCCCAGCAATTA
<i>Pdgfra</i>	GGTCCCAACCTGTAATGAAG	GTAAATGGGACCTGACTTGG
<i>S17</i>	ATGACTTCCACACCAACAAGC	GCCAACTGTAGGCTGAGTGAC
<i>Sox17</i>	GGAATCCAACCAGCCACTG	GGACACCACGGAGGAAATGG
<i>Sox7</i>	CAAGGATGAGAGGAAACGTCTG	TCATCCACATAGGGTCTCTTCTG
<i>Sparc</i>	AGGGCCTGGATCTTCTTTCTC	CAAATTCTCCCATTTCCACCT
<i>Suv39h1</i>	TGTCAACCATAGTTGTGATCC	ATTCCGGTACTCTCCATGTC
<i>Suv39h2</i>	ATCTACGAATGCAACTCAAGGTG	CCACAGCCATTGCTAGTTCTAA
<i>Tbx3</i>	GAACCTACCTGTTCCCGGAAA	CAATGCCCAATGTCTCGAAAAC
<i>Ywhaz</i>	CGTTGTAGGAGCCCGTAGGTCAT	TCTGGTTGCGAAGCATTTGGG

* Primers used in Figure2.

Table S5. Sequences of primers used for ChIP-qPCR

Gene	Forward (5' – 3')	Reverse (5' – 3')	Region
<i>Intergenic</i>	AAGGGGCCTCTGCTTAAAA	AGAGCTCCATGGCAGGTAGA	Control
<i>Vstm2l</i>	GCACGGCTCACAGTACCTAAAGT	CAGCAAGCACGGTGTGTCA	5' TSS
<i>Nnat</i>	CCCTACCCAACCCATCCTATC	CCACCGCGGCACTTTG	Gene body
<i>Esrrb</i>	CTCCCACTCCGCCTTCTC	GGCAAATCACGCGGAAGA	TSS
	GGAAGTGGGAAGTGTGCTAT	GAGCTCCAGATCCCCCTACAC	Enhancer
<i>Klf4</i>	AAGGAAGGCGTTCCAGATTT	TTGAGATCCCTGGTGAAAGG	TSS
	CGCCTGCCTGTACCTTCTAA	GGGCTGGGAGAGATTGTAA	Enhancer
<i>Fgf5</i>	CTCACCAGTCGCAGCTTCT	GAAGGGCTCCACTGGAAACT	TSS
	GTGCATGCATGGGACTGTAG	AACCCGACCTGAACCTAGTG	Enhancer
	TTGGACTGCTGGGGATAGTG	CACGGGGTAAGGTGCTTCTA	Enhancer 1
	GGGGCTTGAGAGTTTCAGAT	AAAGCTCACCTGGCAGTCTA	Enhancer 3
<i>Brachyury</i>	GGCCGACTTTGTTTCTTCCC	GAATGCCTCCTTCTCTCTCA	TSS
	CTCTGTCTCAGTTTGCCATTCTC	TGTACCGACCACTGGAATCC	Enhancer
<i>Zic1</i>	CCCAGTCACAGGAACAGGATA	GGCCGCCACTACAAGAATT	Enhancer

Table S6. Sequences of primers used for H3K9me2 ChIP-qPCR

Gene	Forward (5' – 3')	Reverse (5' – 3')	Region
<i>Brachyury</i>	GGATTCCAGTGGTCGGTACA	AGGCTCTTGGCTCCAGCTAGT	Enhancer
	ACCAAGAACGGCAGGTAGGT	GCTGTAACTCAGCGGGAAG	TSS
	CAAGCCTCCCTGCTGACTT	GGTTCAGCCACTGACACTCA	Control
<i>Fgf5</i>	GCCGACCAGTCTCTTTCATT	TTGCTTCTCCTTCTGCACCT	Enhancer
	GGCTCGGAACATAGCAGTTT	GCCCAAAGGAATCTTGACC	TSS
	GTGTCCCATGGTAACCTGCT	GCAGCCCTGTACAAGATCCA	Control
<i>Magea2</i>	TTGGTGGACAGGGAAGCTAGGGGA	CGCTCCAGAACAAAATGGCGCAGA	TSS

Supplementary Materials and Methods

Generation and rescue of *Jmjd2c*-knockout ESCs

Wild-type JM8-ESC lines from the C57BL/6N mouse background and a mutant ESC line carrying one *Jmjd2c* targeted null allele were obtained from the EUCOMM/IKMC repository (Bradley et al., 2012; Skarnes et al., 2011). The knockout first allele (tm1a) was generated by gene targeting through replacement mutagenesis with a gene-trapping cassette encoding lacZ/ β -galactosidase and a neomycin resistance gene, upstream of a “critical exon” common to all predicted *Jmjd2c* transcripts (Fig. S1A). The generation of biallelic gene targeted cell lines was then carried out through insertional mutagenesis, introducing a second gene-trap cassette through homologous recombination into the second allele (tm2) of *Jmjd2c*, encoding the hygromycin resistance gene and GFP (Fig. S1A) (C. Fisher and W. C. Skarnes, in

preparation). Both cassettes are promoterless, hence relying on the active transcription of *Jmjd2c*, and contain an En2 splice acceptor (SA) signal and the SV40 polyadenylation (pA) sequences to ensure transcripts are spliced into the cassette and stopped at the inserted sites, which is predicted to lead to nonsense mediated decay of these transcripts. FRT sites in the first allele allow the removal of the cassette with FLP recombinase, whereas the loxP sites inserted in the vicinity of the critical exon allow the generation of a conditional null allele with Cre recombinase, however neither of these strategies was used in this study. Validation of the correct insertion of the targeting cassettes was achieved by long-range PCR using the Expand Long Template PCR kit (Roche) with the primers listed in Table S2. Two *Jmjd2c*-knockout clones E2 and E3 were selected for further studies, showing a complete loss of Jmjd2c protein expression as assessed by western blotting. The wild-type (WT) and the two *Jmjd2c*-knockout (*Jmjd2c*-KO) embryonic stem cell clones (E2 and E3) derived from the same parental line were routinely cultured in Knockout-DMEM media (Gibco) supplemented with batch tested 10% fetal bovine serum (FBS), β -mercaptoethanol, L-glutamine, penicillin-streptomycin and LIF (made in house). G418 (100 μ g/mL) and Hygromycin B (25 μ g/mL) were routinely added to the culture medium in the *Jmjd2c*-KO cell lines for selection and removed prior to any experiment.

For rescue of the expression of *Jmjd2c*, the full-length transcript was amplified from the cDNA of WT ESCs and ligated into a pPyCAG-Ires-Puro vector (primer sequences in Table S3). Approximately 3×10^5 *Jmjd2c*-KO clone E3 ESCs were transfected with Lipofectamine 2000 (Invitrogen) and 2 μ g of pPyCAG-Jmjd2c (Rescue) or an empty pPyCAG vectors (Control), then 1 μ g/mL Puromycin (Sigma-Aldrich) was added for selection 24 hours post-transfection. After 8 days of selection individual ESC clones were isolated and expanded.

Generation of *Jmjd2c*-knockdown ESCs

Approximately 10^5 E14Tg2A (E14) ESCs were transfected with Lipofectamine 2000 and 1 μ g of either of two independent shRNA vectors generated against *Jmjd2c* or a control vector as described in Loh et al., 2007. 24 hours post-transfection 1 μ g/mL Puromycin was added for selection and cells harvested after 96 hours of Puromycin selection for subsequent analysis. For generation of stable *Jmjd2c*-knockdown ESC lines, cells were treated 24 hours post-transfection with Puromycin for 8-10 days, colonies picked individually and expanded in GMEM (Gibco) supplemented with 10%

FBS, β -mercaptoethanol, L-glutamine, sodium bicarbonate, sodium pyruvate, non-essential amino acids, penicillin-streptomycin, LIF and Puromycin.

Generation of FV-Jmjd2c ESCs

The full-length *Jmjd2c* transcript was amplified from WT ESCs cDNA and ligated into a pPyCAG-Ires-Puro vector containing a Flag-Flag-V5 at the N-terminal side (primer sequences in Table S3). Approximately 10^6 E14-ESCs were transfected with Lipofectamine 2000 and 4 μ g of Flag-Flag-V5-Jmjd2c (FV-Jmjd2c) or an empty vector (Control). 24 hours post-transfection 1 μ g/mL Puromycin was added for selection and after 8-10 days of culture individual ESC clones were isolated and expanded indefinitely under selection. Cell lines were maintained in GMEM (Gibco) supplemented with 10% FBS, β -mercaptoethanol, L-glutamine, sodium bicarbonate, sodium pyruvate, non-essential amino acids, penicillin-streptomycin, LIF and Puromycin.

Self-renewal assay

To assess the self-renewal ability of ESC populations, 100/cm² cells were seeded in duplicate in serum-containing medium supplemented with LIF. After 5 days the colonies were stained for alkaline phosphatase (AP) activity (Sigma-Aldrich) following the manufacturer's recommendations. Colony morphology was scored as differentiated (<20% stained), mixed (>20%-90% stained), undifferentiated (>90% stained).

Differentiation of ESCs

For induction of embryoid bodies (EBs), 10⁵/cm² cells were cultured in suspension in ultra-low attachment plates (Corning) in ESC media (see Supplemental Materials and Methods) supplemented with 5% FBS without LIF. For all-trans retinoic-acid (atRA) induced differentiation, 2 x 10⁵/cm² cells were seeded in ESC media for 24 hours. Media was then changed into ESC media supplemented with 5% FBS, and 1 μ M of atRA without LIF. EB aggregates and atRA treated cells were collected at the indicated time points for expression analysis, and at day 4 for immunofluorescence staining (atRA assay).

Conversion of ESCs into XEN cells

Conversion of ESCs into XEN cells was performed as described in Niakan et al., 2013. Briefly, 3,000/cm² cells were plated in ESC media. After 24 hours the media was replaced with XEN derivation media: Advanced RPMI (Gibco) with 15% FBS (Biosera), β -mercaptoethanol and penicillin-streptomycin, freshly supplemented with

10 ng/mL Activin A (R&D), 0.01 μ M all-trans retinoic acid (Sigma-Aldrich), 24 ng/mL bFgf (Peprotech) and 1 μ g/mL Heparin (Sigma-Aldrich). After 48 hours of derivation cells were re-plated onto a layer of irradiated MEFs, and maintained in media supplemented with bFgf and Heparin for approximately 10 days. Converted XEN (cXEN) colonies were then manually picked and expanded on 0.1% gelatin coated plates in standard XEN media: Advanced RPMI with 15% FBS, β -mercaptoethanol and penicillin-streptomycin. Embryo-derived XEN^{IM8A} cells (Kunath et al., 2005) were cultured in the same conditions.

Conversion of ESCs into EpiSCs

Conversion of ESCs into EpiSCs was performed as described in Guo et al., 2009. Briefly, ESCs were firstly adapted into serum-free culture conditions in N2B27 (Gibco) medium supplemented with 1 μ M PD0325901 (Mek inhibitor), 3 μ M CHIR99021 (Gsk3 inhibitor) and LIF (in house) for 7 days prior to conversion (Ying et al., 2008). Approximately 5,000/cm² cells were plated in 2i/LIF media on fibronectin-coated plates. After 24 hours the media was changed into N2B27 supplemented with 20 ng/mL Activin A (in house) and 12 ng/mL bFgf (epiblast media). After 10-12 days converted EpiSC (cEpiSC) colonies were detached following incubation with PBS, and expanded in epiblast media in plates coated with 10% FBS. Embryo derived EpiSCs^{Oct4-GiP} (Guo et al., 2009) were cultured in the same conditions.

Mesoderm induction

Converted EpiSCs and embryo-derived EpiSCs were cultured in N2B27 (Guo et al., 2009) or chemically defined media with BSA (CDM-BSA) (Brons et al., 2007), respectively, both supplemented 20 ng/mL Activin A (in house) and 12 ng/mL Fibroblast growth factor (bFgf) (Peprotech). Colonies were dissociated by incubation in PBS and seeded in their respective media at a ratio of 1:6 to 1:10 in plates previously coated with 0.1% gelatin followed by MEF medium (Advanced DMEM/F-12 supplemented with 10% FBS). After 24 hours the media was changed into FLYB media consisting of CDM-PVA supplemented with 20 ng/ μ l bFgf, 10 nM LY294002 (Sigma) and 10 ng/mL BMP4 (R&D). Following 36 hours of mesoderm induction in FLYB conditions, the media was changed into either FB40 – 20 ng/ μ l bFgf and 40 ng/mL BMP4, or FLYWLDN – 20 ng/ μ l bFgf, 2 nM LY294002, 2 ng/mL Wnt3a (Peprotech) and 250 nM LDN193189 (Sigma-Aldrich), for lateral plate mesoderm and paraxial mesoderm differentiation, respectively. Differentiated EpiSCs were

harvested at the indicated time points for expression analysis, and at day 4 for flow cytometry analysis and immunofluorescence staining.

Immunoblotting analysis

Cell lysis was carried out using RIPA buffer (50 mM Tris, 1 mM EDTA, 0.5 mM EGTA, 1% Triton X-100, 0.1% sodium deoxycholate and 140 mM NaCl) supplemented with proteinase and phosphatase inhibitors (Roche). Histones were acid extracted as previously described (Shechter et al., 2007). Protein concentrations of whole cell extracts and acid-extracted histones were measured using a Bradford assay (Thermo Fisher Scientific). The appropriate amounts of whole cell lysates (10-50 µg) or histones (2 µg) were resolved on an 8% or 13% SDS-PAGE gel, respectively, and subsequently transferred into methanol-activated polyvinylidene fluoride membranes (GE Healthcare). Membranes were blocked with 5% skimmed milk (Sigma) for 1 hour and incubated with the appropriate antibodies (see Table S1).

Quantitative PCR

Total RNA was isolated and DNaseI-treated using the RNeasy mini kit (Qiagen). Samples were reverse-transcribed using SuperScript II (Invitrogen) following the manufacturer's instructions. For quantification, cDNA or DNA samples were amplified with Jumpstart SYBR Green PCR Mastermix or KicQstart SYBR Green PCR Mastermix (Sigma), and primer pairs listed in Supplemental Tables S4-S6, using a StepOne™ System (Applied Biosystems). For mesoderm induction RNA extraction was performed with TRIzol (Life Technologies) and samples were reverse transcribed using a QuantiTect Reverse Transcription kit (Qiagen) according to the manufacturer's directions. cDNA was amplified with a QuantiTect SYBR Green PCR kit (Qiagen) and primer pairs listed in Supplemental Table S4, using a Rotor Gene 6000 PCR system (Corbett Life Science).

Immunofluorescence staining

Cells were seeded on gelatinized glass coverslips or 12-well culture plates previously coated with 0.1% gelatin for 10 minutes followed by Advanced DMEM/F-12 with 10% FBS overnight. Cells were fixed in PBS with 4% paraformaldehyde (PFA) for 10 minutes and then permeabilized and blocked at room temperature for 30 minutes using 0.4% Triton X-100 in blocking buffer (10% serum and 90% PBS). Incubation with primary antibody (see Supplemental Table S1) was performed overnight at 4°C, and subsequently incubation with fluorophore-conjugated

secondary antibodies (ThermoFisher) diluted 1:500 for 1 hour at room temperature. Glass coverslips were mounted on Vectashield with DAPI (Vector Laboratories) and visualised using a SP5 Leica laser-scanning confocal microscope or an inverted fluorescent/brightfield microscope.

Flow cytometry analysis

Cells were harvested using cell dissociation buffer (Gibco) and 10^4 cells were blocked in PBS containing 2% FBS, stained for Flk-1 (5 $\mu\text{g/mL}$ anti-Flk-1-Biotin, avas12 a1 clone, eBioscience, followed by 0.4 $\mu\text{g/mL}$ APC-conjugated streptavidin, Biolegend) or Pdgfra (2 $\mu\text{g/mL}$ anti-Pdgfra-PE, clone APA5, eBioscience) and analysed on an Accuri C6 Flow cytometer.

Co-immunoprecipitation

Immunoprecipitation of HA-Flag-G9a (HF-G9a) in fractionated nuclear extracts from HeLa cells was performed as previously described in Fritsch et al., 2010. Briefly, HeLa cell lines expressing a HA-Flag-G9a were generated, together with control cell line expressing an empty vector. Cells were lysed in a hypotonic buffer and disrupted with a Dounce homogenizer, and the cytosolic fraction was separated from nuclei (pellet) by centrifugation. The nuclear soluble and chromatin fractions were separated upon incubation in a high salt buffer followed by centrifugation. The chromatin fraction was further digested with micrococcal nuclease (Sigma-Aldrich). G9a-bound complexes were affinity purified by incubation with anti-Flag antibody bound beads (cat# A2220, Sigma-Aldrich). Complexes were eluted with a Flag peptide (Ansynth) and further purified on anti-HA antibody-conjugated agarose beads (cat# A2095, Sigma-Aldrich) and subsequently eluted with the HA peptide (Ansynth). Co-IPs in nuclear extracts of ESCs were performed as previously described (Battisti et al., 2016). Briefly, cells were lysed similarly as above and nuclei pellets were resuspended in sucrose buffer (20 mM Tris pH 7.65, 60 mM NaCl, 15 mM KCl; 0.34 M Sucrose) followed by an incubation in a high salt buffer (20 mM Tris-HCl pH 7.65, 0.2 mM EDTA, 25% glycerol, 900 mM NaCl, 1.5 mM MgCl_2) resulting in a final NaCl concentration of 300 mM. Nuclear extracts were digested with micrococcal nuclease and sonicated for 10 min (15 sec ON, 45 sec OFF) at high frequency. After pre-clearing, immunoprecipitations were performed overnight at 4°C with the corresponding amount of each antibody or IgG control. Complexes were purified with ultralink beads (Perbio), washed in wash buffer (50 mM Tris-HCl, pH 7.65, 150 mM NaCl, Triton X-100 0.5%) and eluted in NuPAGE® LDS Sample Buffer

(Life Technologies) at 96 °C during 5 min. Immunopurified complexes were resolved on 4-12% SDS-PAGE bis Tris acrylamide gradient gel and immunoblotted with the indicated antibodies (Table S1).

Chromatin immunoprecipitation

In general, chromatin immunoprecipitation (ChIP) of Flag, Jmjd2c, G9a, Med1, Smc1a, Oct4, p300 and H3K27ac followed the procedure described in (Frank et al., 2001), and for H3K9me2 the procedure described in Mozzetta et al., 2014, with the modifications outlined below. Unless stated otherwise, for Jmjd2c, Smc1a, G9a, H3K9me2 ChIPs and Flag-G9a re-ChIPs, cells were fixed with 2 mM Di-Succinimidyl Glutarate (SantaCruz) for 45 minutes at room temperature (Nowak et al., 2005), in addition to an initial 10 minutes fixation step with 1% Formaldehyde (Sigma-Aldrich). Chromatin samples were sonicated on a bioruptor (Diagenode) to produce fragments of 100-500 bp, and ChIPs performed with the antibodies listed in Table S1 and with ProteinG-coupled magnetic Dynabeads (Invitrogen). The amounts of chromatin (DNA or protein) used in each ChIP were as follows: 20 µg of DNA (H3K9me2), 250 µg (G9a), 400 µg (Oct4), 500 µg (Flag, Jmjd2c, p300, H3K27ac) and 800 µg (Med1, Smc1a) of protein. Following washes of bound DNA-protein complexes in the appropriate wash buffers in each referenced protocol, DNA was eluted in 1% SDS at 65°C and treated with 40 ng/µl RNaseA following 0.2 µg/µl Proteinase K. After phenol/chloroform purification, DNA was then precipitated at -20°C with 20-30 µg GlycoBlue carrier (Invitrogen), 1/10 volumes of 3 M NaAc and 2 volumes of 100% ethanol. Resuspended pellets were used for qPCR or for generation of libraries for sequencing. For sequential ChIP (re-ChIP), Flag-bound complexes were eluted at 37 °C for 30 minutes in 75µl of 1% SDS, supplemented with 15mM DTT (Bertero et al., 2015). The eluate was diluted 10 times in the same buffer used for IP and incubated at 4 °C for 5 h, before proceeding to the second round of immunoprecipitations with the G9a antibody, mouse IgG or no antibody ('beads only'). The 'beads only' control was included to normalise for any background from the Flag antibody.

ChIP-sequencing and computational analysis

For sequencing of Flag-Jmjd2c bound DNA fragments, sequencing libraries were prepared using the NEBNext® Ultra™ DNA Library Prep Kit and Multiplex Oligos (New England Biolabs) from 5 ng of DNA. Following analysis on an Agilent Bioanalyzer libraries were pooled and sequenced on an Illumina Genome Analyzer II (Illumina). Quality of the sequenced reads was assessed using the FASTQC

program (Babraham Bioinformatics). Reads were aligned to the UCSC mouse reference genome (mm9) using Bowtie2 (Langmead and Salzberg, 2012), and only uniquely aligned reads were retained. Aligned reads (SAM) were converted into BED format to subsequently generate bigwig files for visualization in the IGV browser (Robinson et al., 2011). For each condition (2i/LIF and serum/LIF), the input and two biological duplicates were sequenced. Due to the high correlation between bigwig files of each pair of replicates, individual BAM files were merged and used in peak calling. List of enriched peaks were obtained using MACS2 with an FDR <0.0001 by calling peaks relative to the respective input control samples (background). Gene annotation to the nearest TSS and motif enrichment analysis was performed using HOMER (Heinz et al., 2010), respectively. For the charts in Figure S8D, the same treatment was applied to the ChIP-seq profiles referenced. Density plots and heatmaps in Figure 3C,E and Figure 5A were generated with deepTools (Ramirez et al., 2014). Overlaps between two genomic intervals were identified with the Intersect function in usegalaxy.org (Blankenberg et al., 2010; Giardine et al., 2005; Goecks et al., 2010). Counts for generation of Venn Diagrams in Figure 5B between three datasets were obtained using the R package ChiPpeakAnno (Zhu et al., 2010). To identify the functional classification listed on Figure 3G, Jmjd2c-bound H3K27-low genomic regions were inputted into GREAT (Genomic Regions Enrichment of Annotations Tool) and tested against the mouse genome (McLean et al., 2010). For the analysis in Figure 4, S9 and S10 ChIP-seq data were downloaded from Genome Expression Omnibus (GEO) as SRA files, converted to FASTQ format using fastq-dump.2.4.2, evaluated using FASTQC program (Babraham Bioinformatics), trimmed and filtered using Trimmomatic-0.33 (LEADING:10 TRAILING:10 SLIDINGWINDOW:4:18 MINLEN:20) (Bolger et al., 2014). Sequences were aligned to the mm9 version of the mouse genome using Bowtie2. To calculate the average ChIP-seq read coverage at Jmjd2c-bound sites, BAM files were read into R, duplicate reads were removed and the bam files were converted to coverage objects using the Genomic Alignments package (Lawrence et al., 2013). The coverage objects were normalised to both sequencing depth and their respective inputs as follows:

$$F = 10^6/T$$

$$N_s = CF$$

$$N = \frac{N_s}{I}$$

Where T is the total number of reads, F is the sequencing depth normalisation factor, C is the pre-normalised read coverage, N_s is the sequencing depth normalised read coverage, I is the input read coverage and N is the sequence read and input normalised read coverage.

Coverage heatmaps were generated using the gplots package (Zhang, 2016). To plot the coverage heatmaps values greater than 3 standard deviations from the mean were removed and replaced values imputed by the mice R package. The largest number of values replaced from a single dataset was 69 out of 10,000 (0.7%). Pearson correlation coefficients of the average read coverage were calculated and visualised as heatmaps.

The accession numbers of the published ChIP-seq datasets analysed are listed below. Raw or treated files were obtained directly from the GEO repository, the mouse ESC ChIP-seq compendium (Martello et al., 2012) or the Supplementary Information of the referenced paper. For G9a, bigwig files were generated using the parameters described in Mozzetta et al., 2014.

Accession	Reference	Factor	BED files	BigWig files
GSE11724	Marson et al., 2008	Oct4	Kagey et al., 2010	Compendium
GSE22562	Kagey et al., 2010	Med1	Kagey et al., 2010	Compendium
GSE22562	Kagey et al., 2010	Smc1a	Kagey et al., 2010	Compendium
GSE24165	Creyghton et al., 2010	p300	Creyghton et al., 2010	Compendium
GSE46536	Mozzetta et al., 2014	G9a	GEO	Generated
GSE43229	Das et al., 2014	Jmjd2c	Generated	Generated
GSE53936	Pedersen et al., 2014	Jmjd2c	Generated	Generated
GSE48519	Hon et al., 2014	H3K4me1	-	GEO
GSE48519	Hon et al., 2014	H3K27ac	-	GEO
GSE48519	Hon et al., 2014	H3K4me3	-	GEO
GSE27827	Lienert et al., 2010	H3K4me2	-	GEO
GSE54412	Liu et al., 2015	H3K9me2	-	Generated
GSE43229	Das et al., 2014	H3K9me2	-	Generated

RNA-seq analysis

RNA-seq was treated as described above and were aligned to the mm9 version of the mouse genome using tophat-2.1.0 (Trapnell et al., 2009). Transcript assembly and differential expression analysis was performed using the cufflinks-2.2.1 suite of

software (Trapnell et al., 2013; Trapnell et al., 2010). TopHat aligned reads were assembled using Cufflinks, the final transcriptome assembly was generated using Cuffmerge and differential expression was evaluated using Cuffdiff. Chi-square tests were performed on the Cuffdiff evaluated differentially expressed gene lists. The genes were divided into Jmjd2c-G9a regulated and all other annotated genes. Up and downregulated genes were defined as those with statistically significant (q -value <0.05) log2 fold-changes in expression between the G9a-knockout and wild-type cells. Non-differentially expressed genes were defined as those with a non-significant change in expression (q -value >0.05). The functional classification of both sets of genes was identified through a statistical enrichment test using default settings in PantherDB GO (Mi et al., 2013).

Capture Hi-C in ESCs

To identify integration profile for promoter of *Foxa2* in Figure S13, the CHiCAGO pipeline was used to output scores for capture Hi-C data from the study Joshi et al., 2015. A manuscript on the CHiCAGO pipeline (Cairns et al., 2016) is publically available, with the pipeline itself at regulatorygenomicsgroup.org/chicago. Probe targeted Dpn2 fragments from *Foxa2* gene promoter were used as regions of interest and interactions anchored at the same region, with a threshold CHiCAGO score of 5 were considered. For further information on capture Hi-C or interaction calling and scoring please refer to (Joshi et al., 2015) and (Cairns et al., 2016).

Supplementary References

- Battisti, V., Pontis, J., Boyarchuk, E., Fritsch, L., Robin, P., Ait-Si-Ali, S. and Joliot, V.** (2016). Unexpected Distinct Roles of the Related Histone H3 Lysine 9 Methyltransferases G9a and G9a-Like Protein in Myoblasts. *J Mol Biol* **428**, 2329-2343.
- Bertero, A., Madrigal, P., Galli, A., Hubner, N. C., Moreno, I., Burks, D., Brown, S., Pedersen, R. A., Gaffney, D., Mendjan, S., et al.** (2015). Activin/nodal signaling and NANOG orchestrate human embryonic stem cell fate decisions by controlling the H3K4me3 chromatin mark. *Genes Dev* **29**, 702-717.
- Blankenberg, D., Von Kuster, G., Coraor, N., Ananda, G., Lazarus, R., Mangan, M., Nekrutenko, A. and Taylor, J.** (2010). Galaxy: a web-based genome analysis tool for experimentalists. *Curr Protoc Mol Biol* **Chapter 19**, Unit 19 10 11-21.

- Bolger, A. M., Lohse, M. and Usadel, B.** (2014). Trimmomatic: a flexible trimmer for Illumina sequence data. *Bioinformatics* **30**, 2114-2120.
- Brons, I. G., Smithers, L. E., Trotter, M. W., Rugg-Gunn, P., Sun, B., Chuva de Sousa Lopes, S. M., Howlett, S. K., Clarkson, A., Ahrlund-Richter, L., Pedersen, R. A., et al.** (2007). Derivation of pluripotent epiblast stem cells from mammalian embryos. *Nature* **448**, 191-195.
- Cairns, J., Freire-Pritchett, P., Wingett, S. W., Varnai, C., Dimond, A., Plagnol, V., Zerbino, D., Schoenfelder, S., Javierre, B. M., Osborne, C., et al.** (2016). CHiCAGO: robust detection of DNA looping interactions in Capture Hi-C data. *Genome Biol* **17**, 127.
- Frank, S. R., Schroeder, M., Fernandez, P., Taubert, S. and Amati, B.** (2001). Binding of c-Myc to chromatin mediates mitogen-induced acetylation of histone H4 and gene activation. *Genes Dev* **15**, 2069-2082.
- Giardine, B., Riemer, C., Hardison, R. C., Burhans, R., Elnitski, L., Shah, P., Zhang, Y., Blankenberg, D., Albert, I., Taylor, J., et al.** (2005). Galaxy: a platform for interactive large-scale genome analysis. *Genome Res* **15**, 1451-1455.
- Goecks, J., Nekrutenko, A., Taylor, J. and Galaxy, T.** (2010). Galaxy: a comprehensive approach for supporting accessible, reproducible, and transparent computational research in the life sciences. *Genome Biol* **11**, R86.
- Guo, G., Yang, J., Nichols, J., Hall, J. S., Eyres, I., Mansfield, W. and Smith, A.** (2009). Klf4 reverts developmentally programmed restriction of ground state pluripotency. *Development* **136**, 1063-1069.
- Heinz, S., Benner, C., Spann, N., Bertolino, E., Lin, Y. C., Laslo, P., Cheng, J. X., Murre, C., Singh, H. and Glass, C. K.** (2010). Simple combinations of lineage-determining transcription factors prime cis-regulatory elements required for macrophage and B cell identities. *Mol Cell* **38**, 576-589.
- Joshi, O., Wang, S. Y., Kuznetsova, T., Atlasi, Y., Peng, T., Fabre, P. J., Habibi, E., Shaik, J., Saeed, S., Handoko, L., et al.** (2015). Dynamic Reorganization of Extremely Long-Range Promoter-Promoter Interactions between Two States of Pluripotency. *Cell Stem Cell* **17**, 748-757.
- Langmead, B. and Salzberg, S. L.** (2012). Fast gapped-read alignment with Bowtie 2. *Nat Methods* **9**, 357-359.

- Lawrence, M., Huber, W., Pages, H., Aboyoun, P., Carlson, M., Gentleman, R., Morgan, M. T. and Carey, V. J.** (2013). Software for computing and annotating genomic ranges. *PLoS Comput Biol* **9**, e1003118.
- Martello, G., Sugimoto, T., Diamanti, E., Joshi, A., Hannah, R., Ohtsuka, S., Gottgens, B., Niwa, H. and Smith, A.** (2012). Esrrb is a pivotal target of the Gsk3/Tcf3 axis regulating embryonic stem cell self-renewal. *Cell Stem Cell* **11**, 491-504.
- McLean, C. Y., Bristor, D., Hiller, M., Clarke, S. L., Schaar, B. T., Lowe, C. B., Wenger, A. M. and Bejerano, G.** (2010). GREAT improves functional interpretation of cis-regulatory regions. *Nat Biotechnol* **28**, 495-501.
- Mi, H., Muruganujan, A., Casagrande, J. T. and Thomas, P. D.** (2013). Large-scale gene function analysis with the PANTHER classification system. *Nat Protoc* **8**, 1551-1566.
- Nowak, D. E., Tian, B. and Brasier, A. R.** (2005). Two-step cross-linking method for identification of NF-kappaB gene network by chromatin immunoprecipitation. *Biotechniques* **39**, 715-725.
- Ramirez, F., Dundar, F., Diehl, S., Gruning, B. A. and Manke, T.** (2014). deepTools: a flexible platform for exploring deep-sequencing data. *Nucleic Acids Res* **42**, W187-191.
- Robinson, J. T., Thorvaldsdottir, H., Winckler, W., Guttman, M., Lander, E. S., Getz, G. and Mesirov, J. P.** (2011). Integrative genomics viewer. *Nat Biotechnol* **29**, 24-26.
- Shechter, D., Dormann, H. L., Allis, C. D. and Hake, S. B.** (2007). Extraction, purification and analysis of histones. *Nat Protoc* **2**, 1445-1457.
- Trapnell, C., Hendrickson, D. G., Sauvageau, M., Goff, L., Rinn, J. L. and Pachter, L.** (2013). Differential analysis of gene regulation at transcript resolution with RNA-seq. *Nat Biotechnol* **31**, 46-53.
- Trapnell, C., Pachter, L. and Salzberg, S. L.** (2009). TopHat: discovering splice junctions with RNA-Seq. *Bioinformatics* **25**, 1105-1111.
- Trapnell, C., Williams, B. A., Pertea, G., Mortazavi, A., Kwan, G., van Baren, M. J., Salzberg, S. L., Wold, B. J. and Pachter, L.** (2010). Transcript assembly and quantification by RNA-Seq reveals unannotated transcripts and isoform switching during cell differentiation. *Nat Biotechnol* **28**, 511-515.

- Zhang, Z.** (2016). Multiple imputation with multivariate imputation by chained equation (MICE) package. *Ann Transl Med* **4**, 30.
- Zhu, L. J., Gazin, C., Lawson, N. D., Pages, H., Lin, S. M., Lapointe, D. S. and Green, M. R.** (2010). ChIPpeakAnno: a Bioconductor package to annotate ChIP-seq and ChIP-chip data. *BMC Bioinformatics* **11**, 237.